Chronic *Staphylococcus aureus* infection is cured by theory-driven therapy

Lito A. Papaxenopoulou,[1]* Gang Zhao,[1] Sahamoddin Khailaie,[1] Konstantinos Katsoulis-Dimitriou,[2] Ingo Schmitz,[2,3,4] Eva Medina,[5] Haralampos Hatzikirou,[1,6,7]* Michael Meyer-Hermann[1,8,9]*

[1] Department of Systems Immunology and Braunschweig Integrated Centre of Systems Biology, Helmholtz Centre for Infection Research, 38106, Braunschweig, Germany.

[2] Institute for Molecular and Clinical Immunology, Medical Faculty, Otto-von-Guericke-University, 39120, Magdeburg, Germany.

[3] Systems-oriented Immunology and Inflammation Research Group, Department of Experimental Immunology, Helmholtz Centre for Infection Research, 38124, Braunschweig, Germany.

[4] Department of Molecular Immunology, ZKF2, Medical Faculty, Ruhr-University Bochum, 44780, Bochum, Germany

[5] Department of Infection Immunology, Helmholtz Centre for Infection Research, 38124, Braunschweig, Germany.

[6] Technische Univesität Dresden, Center for Information Services and High Performance Computing, 01062, Dresden, Germany.

[7] Mathematics Department, Khalifa University, P.O. Box: 127788, Abu Dhabi, UAE.

[8] Institute for Biochemistry, Biotechnology and Bioinformatics, Technische Universität Braunschweig, 38106, Braunschweig, Germany.

[9] Centre for Individualised Infection Medicine (CiiM), 30625, Hannover, Germany.

*Correspondence: papaxenopoulou.lito@gmail.com (LP); haralampos.hatzikirou@ku.ac.ae (HH); mmh@theoretical-biology.de (MMH).

SUMMARY

Staphylococcus aureus is considered a dangerous pathogen due to its ability to evade the immune system and resist multiple antibiotics. These evasive strategies lead to difficult-to-treat chronic infections and abscesses in internal organs including kidneys, which are associated with the expansion of myeloid-derived suppressor cells (MDSCs) and their suppressive effect on T cells. Here, we developed a mathematical model of chronic *S. aureus* infection that incorporates the T-cell suppression by MDSCs and suggests therapeutic strategies to eradicate *S. aureus*. We quantified *in silico* a therapeutic protocol with heat-killed *S. aureus* (HKSA), which we tested *in vivo*. Contrary to conventional administration of heat-killed bacteria as vaccination prior to infection, we administered HKSA as treatment, when the hosts were already chronically infected. Our treatment cured all chronically *S. aureus*-infected mice, reduced MDSCs, and reversed T-cell dysfunction by inducing acute inflammation during ongoing, chronic infection without any use of standard treatments that involve antibiotics, MDSC-targeting drugs (chemotherapy), or procedures such as abscess drainage. This study is a proof-of-principle for a treatment protocol against chronic *S. aureus* infection and renal abscesses by repurposing heat-killed treatments, guided and quantified by mathematical modelling. Our mathematical model further explains why previous treatment with inactivated *S. aureus* administered to long-term infected human patients has not led to cure. Overall, our results can have direct relevance to the design of human therapeutics against chronic *S. aureus* infections.

In brief: A theory-driven treatment protocol with heat-killed *S. aureus* eradicates *S. aureus,* reduces MDSCs, and reverses T-cell dysfunction *in vivo*.

Graphical abstract

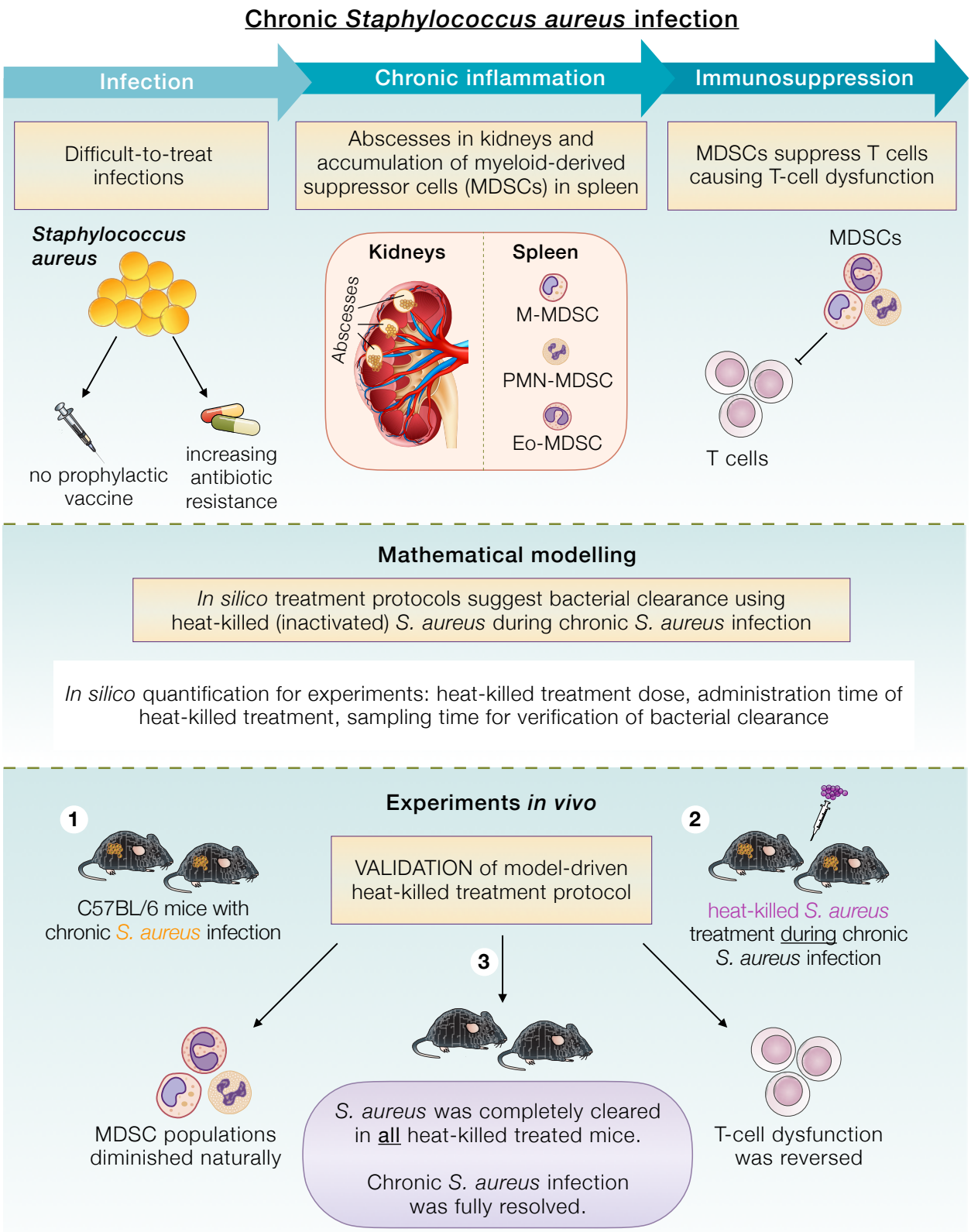

47 **Keywords**

48 Chronic *Staphylococcus aureus* infection, mathematical model, myeloid-derived suppressor cells
49 (MDSCs), chronic bacterial infection, model-driven experiments, heat-killed treatment, *S. aureus*
50 infection cured, sterilizing immunity.

51
52 **INTRODUCTION**

53 *Staphylococcus aureus* is a bacterial human pathogen colonizing 20%-30% of the world
54 population and is responsible for nosocomial-acquired and community-acquired infections.
55 Colonization by *S. aureus* as a commensal bacterium is non-problematic. However, after a skin
56 cut, surgery or implantation of medical devices, *S. aureus* can reach deeper tissues and cause
57 life-threatening conditions like pneumonia, endocarditis, osteomyelitis and abscesses in internal
58 organs (*1*, *2*).

59 The pathogen is of substantial medical concern because it can infect any organ in the
60 body (*1*, *2*), even without being disseminated via the bloodstream (*3*). Moreover, its multiple
61 mechanisms to manipulate and evade immune defenses along with its increasing antibiotic-
62 resistance lead to its persistence in the host and cause chronic, difficult-to-treat infections (*4*).
63 The urgency for new treatments aiming at curing *S. aureus* infections is also emphasized by the
64 WHO, which, on its global priority list of infectious agents, identified *S. aureus* as a "high-
65 priority" pathogen.

66 Chronic *S. aureus* infections such as chronic osteomyelitis, recurrent furunculosis, and
67 abscesses are hard to eliminate. We have previously shown that during the *chronic phase* of *S.*
68 *aureus* infection, effectors of innate immunity, such as macrophages (MΦ) and neutrophils, as
69 well as B cells are dispensable for bacterial containment, unlike T cells, which are critical for
70 bacterial control (*5*). However, T cells fail to eradicate the pathogen because prolonged antigenic

71 stimulation (confluent with chronic infection) causes them to enter an anergic state that seems to
72 be irreversible (*5*). As we demonstrated, T-cell dysfunction (also known as T-cell anergy, T-cell
73 suppression, or T-cell hyporesponsiveness) during chronic *S. aureus* infection is attributed to
74 myeloid-derived suppressor cells (MDSCs) rather than other immunosuppressive cells such as
75 regulatory T and B cells, or tolerogenic dendritic cells (*6*).

76 MDSCs constitute a heterogeneous population of immature myeloid cells that expand in
77 long-lasting pathological conditions, such as chronic bacterial and viral infections (*7*, *8*)
78 including severe SARS-CoV-2 infection (*9*), cancer (*10*), and autoimmunity (*11*). Expansion of
79 MDSCs serves as a natural, anti-inflammatory response to mitigate the detrimental effect of
80 prolonged inflammation (*12*). Often pathogens exploit the immunosuppressive effect by MDSCs
81 to persist within the host, thus establishing chronic infections (*12*). MDSCs are distinguished in
82 three subsets that share the capacity to suppress T cells during chronic *S. aureus* infection:
83 monocytic $CD11b^{+}Ly6C^{+}Ly6G^{low}$, granulocytic/neutrophilic
84 $CD11b^{+}Ly6C^{low}Ly6G^{+}$ and eosinophilic $CD11b^{+}Ly6C^{low}Ly6G^{low}$ MDSCs, known as M-
85 MDSC, PMN-MDSC and Eo-MDSC respectively (*6*, *8*, *13*).

86 Despite much research, there is no *S. aureus* vaccine to confer prophylaxis against *S.*
87 *aureus* infections and along with antibiotic-resistance, *S. aureus* is becoming increasingly
88 dangerous every year. It has been estimated that in 2001 *S. aureus* infections afflicted 292045
89 US hospital inpatients, caused almost 12000 inpatient deaths and cost $9.5 billion in excess
90 charges in US hospitals alone (*14*). By 2014, the number of US inpatients afflicted with
91 methicillin-susceptible and methicillin-resistant *S. aureus* alone has risen dramatically to 616070
92 individuals and associated costs were estimated to be around $14.6 billion (*15*). Abscesses
93 caused by antibiotic-resistant *S. aureus* have also been increasing. Current treatments rely on

94 simultaneous use of various antibiotics (which promote antibiotic resistance), MDSC-targeting
95 drugs (which are cytotoxic and can have side-effects), and surgery to drain abscesses. Renal
96 abscesses in particular are highly destructive and when multiple antibiotics and abscess drainage
97 fail, immediate nephrectomy is required to save a patient's life (*16*). Consequently, finding new
98 treatments against *S. aureus* infections is absolutely essential.

99 Experimental investigations have offered important information on mechanisms of
100 bacterial persistence or MDSC-mediated immunosuppression, however, how to intervene in the
101 complex balance between bacteria, T cells and MDSCs during chronic *S. aureus* infections in
102 order to cure, remains obscure. In this study we constructed a mathematical model to understand
103 the balance between immunity and *S. aureus* during chronic infection and to explore strategies
104 that could cure the infection. Modelling the chronic infection mathematically could bestow a
105 broader observation of possible treatments that would be challenging to discover only by
106 experimental means, whereas *in silico* they could expeditiously and cost-effectively be tested for
107 rendering sterilizing immunity. Mathematical models have been used to shed light on *S. aureus*
108 transmission in community and hospitals (*17*, *18*), staphylococcal growth on foods (*19*),
109 interactions of the pathogen and immune cells during the acute phase of infection (*20*), but also
110 to suggest the optimal sequence of antibiotic administration that could reduce the virulence of *S.*
111 *aureus* (*21*). However, there are still large gaps on chronic *S. aureus* infections and how to cure
112 them. To our knowledge, this is the first mathematical model that investigates the dynamics of
113 *chronic S. aureus* infection between bacteria and T cells, in the presence of MDSCs, and
114 suggests curative treatments.

115 Our *in silico* analysis suggested various strategies that could perturb the dynamics of the
116 chronic infection system and cure the infection. For experimental testing *in vivo*, we quantified *in*

117 *silico* a dose-day treatment protocol using heat-killed (HK), namely inactivated, bacteria. Unlike
118 prior vaccination with HK *S. aureus* (HKSA), which is meant as prophylaxis but instead fails to
119 eradicate the pathogen and exacerbates the infection (*22*), we administered HKSA as treatment,
120 when the hosts were already chronically *S. aureus*-infected. Our *in silico* therapeutic protocol
121 was validated *in vivo*. We here report for the first time reversion of T-cell dysfunction, MDSC-
122 reduction and eradication of *S. aureus* in all HKSA-treated mice without any use of antibiotics,
123 MDSC-targeting drugs, or procedures such as abscess drainage. Our experiments further verified
124 that our HKSA protocol triggered acute inflammation during the already established chronic *S.*
125 *aureus* infection, which served as the perturbation of the system dynamics and cured the
126 infection. The therapeutic effect of heat-killed treatment is not limited to HKSA, because
127 treatment with heat-killed *Streptococcus pyogenes* (HKSP) also cured a portion of treated
128 animals, reverted T-cell dysfunction and induced acute inflammation during ongoing chronic *S.*
129 *aureus* infection. Our study is a proof-of-principle for a treatment protocol against chronic *S.*
130 *aureus* infection and renal abscesses by repurposing heat-killed administration, guided and
131 quantified by mathematical modelling that can have direct relevance to the design of human
132 therapeutics against chronic *S. aureus* infections and abscesses in internal organs.
133

RESULTS

Dynamics of chronic infection

We have previously shown that intravenous inoculation with *S. aureus* results in chronic infection and abscesses in kidneys (*5*, *6*). Bacterial containment in the chronic phase of infection is not attributed to innate immune cells but mainly to effector $CD4^+$ T cells, which gradually lose functionality due to suppression by MDSCs (*5*, *6*). Here, we constructed a mathematical model that includes the above-mentioned interactions between bacteria B(t), T cells T(t), and T-cell suppression by MDSCs (Θ) during *chronic S. aureus* infection. In the following the term T cells will refer to $CD4^+$ T cells unless otherwise stated.

The ordinary differential equation (ODE) system reads

$$\dot{B}(t) = r_b B(t)\left(1 - \frac{B(t)}{\kappa}\right) - c_b T(t) B(t), \qquad (1)$$

$$\dot{T}(t) = r_t T^2(t)\left(1 - \frac{T(t)}{K_T}\right) + k_b B(t) - c_T B(t) T(t) - \Theta\, T(t), \qquad (2)$$

where a dot represents differentiation with respect to time.

During infection, *S. aureus* uses various mechanisms to persist within the host (*23*). This is represented with the term $r_b B(t)(1-B(t)/\varkappa)$ capturing bacterial expansion by logistic growth. Staphylococcal presence stimulates T cells (term $k_b B(t)$), which proliferate (term $r_t T^2(t)$). T-cell proliferation is represented with the term $r_t T^2(t)$ because activated T cells secrete Interleukin-2 (IL-2), which induces cell cycle progression of T cells. In return, it creates a positive feedback loop for T-cell proliferation, and hence the term $r_t T^2(t)$ as we reported previously (*24*). The term $(1-T(t)/K_T)$ describes the carrying capacity of T cells. As infection becomes chronic, T cells

154 contain bacteria (term $c_b T(t)B(t)$) (*5*). However, bacterial persistence causes chronic (long-
155 lasting) inflammation, which is harmful to the host. To protect from the adverse effect of
156 prolonged inflammatory signal, MDSCs gradually expand to suppress T-cell activity (*6*). T-cell
157 suppression by MDSCs can happen *systemically,* namely distantly from the site of infection such
158 as in the spleen *(6, 13)*, where T cells increase substantially during chronic *S. aureus* infection
159 (*5*). This is represented with the term $\Theta\ T(t)$, since MDSC-mediated immunosuppression on T
160 cells requires direct cell–cell contact or cell–cell proximity (*6*). *Locally*, namely at the site of
161 infection, the pathogen can exploit MDSCs towards T-cell suppression to promote its persistence
162 (term $c_T B(t)T(t)$) *(12)*. A schematic representation of the model is illustrated in Fig. 1A. It is
163 important to note that although innate immune responses do not explicitly appear in the
164 equations, they were not ignored but were rather indirectly incorporated into the term describing
165 bacterial growth, $r_b B(t)(1-B(t)/\varkappa)$ (Eq. (1)). In particular, model parameters were identified with
166 the use of our previously reported experimental results from T and B cells-deficient RAG2$^{-/-}$
167 mice (only innate immunity present) and immunocompetent mice with chronic *S. aureus*
168 infection and renal abscesses (*5*) (full description in Supplementary Materials). We previously
169 reported major T-cell suppression by MDSCs in spleens of mice with local, chronic *S. aureus*
170 infection in kidneys (*6*, *13*). This phenomenon is known as extramedullar haematopoiesis,
171 happens during chronic inflammation and involves haematopoiesis mostly in spleen, which
172 further induces accumulation of MDSCs in the organ (*25*). In accordance, our fitting revealed
173 that parameter c_T describing local T-cell suppression by MDSCs in kidneys (the site of
174 infection), was negligible compared to parameter Θ describing systemic T-cell suppression by
175 MDSCs, such as in spleens (Supplementary Materials).

176 We previously demonstrated experimentally that during chronic *S. aureus* infection there
177 is substantial negative correlation between MDSC populations and activated T cells, which are
178 not suppressed (dysfunctional) and hence maintain their ability to proliferate (*6*). To validate the
179 accuracy and consistency of our mathematical model, we reproduced the inverse proportional
180 behaviour between T cells and T-cell suppression by MDSCs (Fig. 1B). Further *in silico* analysis
181 showed how chronic *S. aureus* infection is established naturally, without any treatment
182 intervention (Fig. 1C). Infection induces strong inflammation, which activates T cells.
183 Competition for dominance between bacteria and T cells creates oscillations in the population
184 dynamics (Fig. 1C). To protect from the damaging effect of prolonged inflammation, MDSCs
185 expand gradually to suppress T cells. Increasing accumulation of MDSCs leads to increasing
186 suppression on T cells (Θ). Upon a critical threshold, T-cell suppression by MDSCs is so strong
187 that T cells become dysfunctional and cannot promote sterilizing immunity anymore (Fig. 1D,
188 *pink line*). This *in silico* result agrees with our previous experimental observations, showing that
189 gradual expansion of MDSCs leads to gradual loss of T-cell function, which in turn promotes
190 chronic *S. aureus* infection and failure of sterilizing immunity (*5*, *6*). At this point the immune
191 system finds the balance between maximal bacterial clearance and minimal collateral tissue
192 damage, whereas bacteria persist in the host organism but are simultaneously unable to further
193 grow due to their containment by T cells (*5*) (mathematically known as equilibrium of the
194 system). This equilibrium is found to be stable by our mathematical model (Fig. 1E) and
195 biologically refers to chronic *S. aureus* infection. Once at this stage (Fig. 1D, *pink line;* 1E),
196 sterilizing immunity can be attained only by using treatment-interventions that can destabilize
197 (i.e. perturb) this stable steady state of chronic infection.

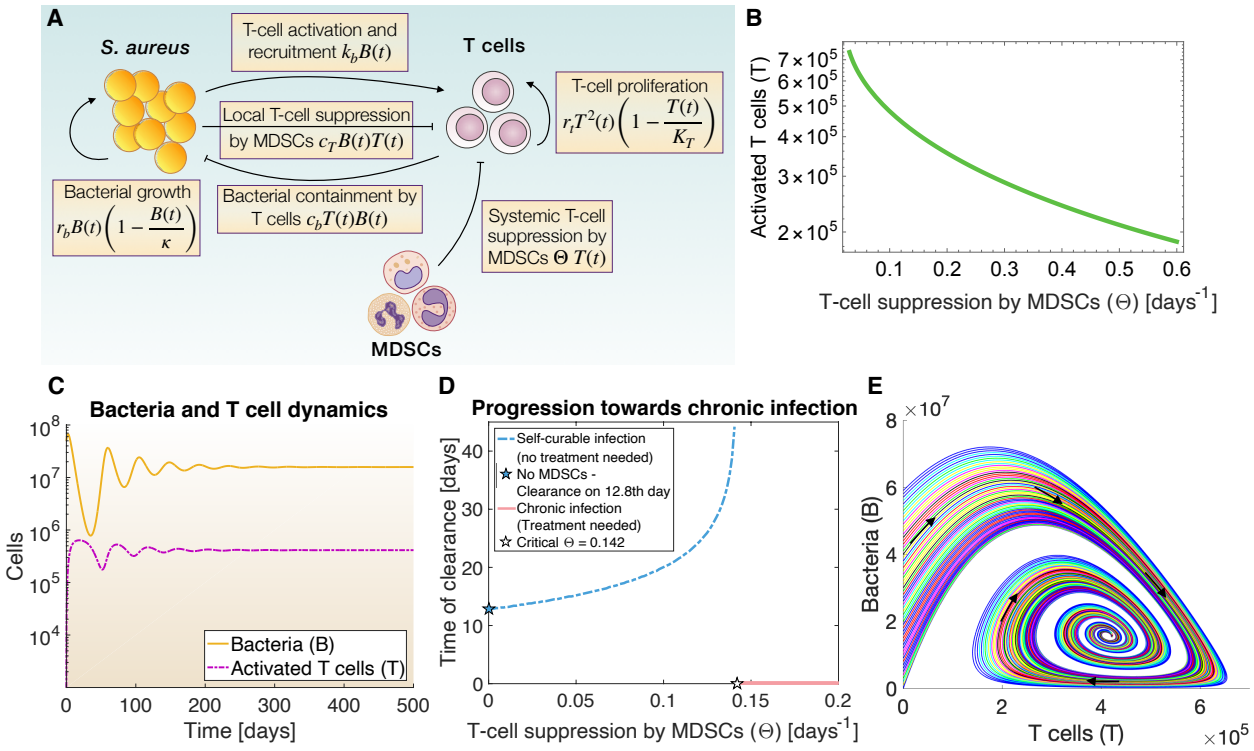

Fig. 1. Dynamics of chronic *Staphylococcus aureus* infection. (**A**) Schematic representation of chronic *S. aureus* infection model. (**B**) Correlation between T cells and T-cell suppression by MDSCs (Θ) is inversely proportional. The correlation was plotted using the analytical solutions of the T-cell differential equation in steady state (Supplementary Materials, Eq. (S5)) for increasing values of parameter Θ. (**C**) Dynamics of bacteria (B) and activated T cells (T) in time are shown as numerical solutions of the ODE system. Infection was induced by setting the bacterial population equal to 5×10^7 cells at day 0 in Eq. (1) to be consistent with experimental bacterial inoculation causing chronic *S. aureus* infection (*6*). Model parameters are as shown in table S1. (**D**) Infection was initiated as in (**C**). Numerical calculation of bacteria for changing values of parameter Θ (T-cell suppression by MDSCs) in the range [0, 0.2]. For bacterial numbers <0.000001, the infection is considered cured (blue), else persisting (pink) and the corresponding day of bacterial clearance is shown or set to zero, respectively. The blue star represents a scenario of MDSC-absence and hence non-existent T-cell suppression (Θ=0). As Θ gradually increases, the infection progresses towards

212 chronic phase and bacterial clearance becomes more difficult. The blue line represents when, despite
213 MDSC-mediated suppression, the infection can be cured by the immune response alone. The white
214 star represents the critical value of Θ, when T cells become anergic by MDSC-mediated suppression,
215 the infection persists and external treatment-intervention is required for cure. Table S1 shows the
216 values for the rest of the model parameters. (**E**) Stable steady state of ODE system between bacteria
217 and T cells. For changing initial numbers of bacteria in the range [10^5, 6×10^7) at day 0, the system
218 always terminates in stable equilibrium, which biologically corresponds to the chronic infection.
219 Black arrows illustrate the flow of the system. Model parameters are shown in table S1.

220

221 **Model-driven therapeutic strategies**

222 To explore perturbation strategies (treatments) that would destabilize the equilibrium between
223 bacteria, T cells and MDSCs, we varied values of k_b and Θ. These parameters, representing T-
224 cell activation and recruitment by bacterial presence, and T-cell suppression by MDSCs,
225 respectively, were specifically chosen because they play a key role in the establishment of
226 chronic infection (*5*, *6*). Different values of k_b and Θ gave different eigenvalues for the ODE
227 system (Eqs. (1)-(2)), which were used to characterize the steady states (equilibria) of the
228 mathematical model as unstable or stable (analytical forms are found in Supplementary
229 Materials). Combining *in silico* all steady states in one separatrix (phase diagram) led to the
230 distinguished areas of cure and chronic infection (Fig. 2A).

231 To gain more understanding of the dynamical system and suggest strategies for bacterial
232 clearance, we next estimated the average position of an infected host on the separatrix of cure
233 and chronic infection (Fig. 2A, *white star*), using the values of parameters k_b and Θ as fitted
234 previously (table S1). We found that it lay in the region of chronic infection, yet close to the

235 basin of attraction (region) of cure. According to the separatrix, we concluded that the resolution
236 of chronic infection is achieved via either (a) relocation of the infected host from the chronic
237 infection area towards the area of cure (Fig. 2A) by (i) increasing T-cell activation and
238 recruitment (k_b) and/or by (ii) decreasing T-cell suppression by MDSCs (Θ) or (b) via expansion
239 of the cure zone itself (Fig. 2B) by counter-intuitively (iii) increasing the proliferation rate of
240 bacteria (r_b) and/or (iv) by reducing bacterial containment by T cells (c_b). These *in silico* results
241 accord with previous experimental studies reporting that brief suppression of immunity (namely
242 c_b reduction) with cyclophosphamide (*3*) or targeting MDSCs (namely Θ decrease) (*26*) during
243 *S. aureus* infection reduce bacterial burden. Altogether the model indicates that all four
244 aforementioned perturbation categories (each of which can be implemented *in vivo* in various
245 ways) can destabilize the dynamics of chronic infection so that eradication of *S. aureus* and
246 *sterilizing immunity* is achieved (fig. S1).
247
248 **Design of quantitative, model-driven experiments**
249 Our *in silico* analysis suggested treatment strategies that were MDSC-targeting (Θ decrease),
250 pathogen-targeting (r_b increase or c_b decrease), or host-directed (k_b increase). Experimental
251 testing was essential to validate the model predictions. Since validation of bacterial eradication
252 would have immense importance for human therapeutics, we sought to test experimentally a
253 treatment that would be safe and easy to apply.
254 MDSC-targeting drugs, such as gemcitabine chemotherapeutic agent, usually bear
255 adverse side-effects because of their cytotoxicity. They simultaneously deplete mature immune
256 cells (*26*), which are indispensable components of immunity. Furthermore, available MDSC-
257 targeting drugs fail to eliminate MDSCs in many organs (*27*). Lastly, the heterogeneity of

258 MDSCs makes it particularly difficult to identify a single drug that would deplete all distinct
259 MDSC subsets, each of which is linked to different bacterial infections and even distinct tumors
260 (*8*, *28*).

261 Contrary to conventional bacteria-targeting drugs, such as antibiotics, that aim at fighting
262 bacteria and whose use should be limited because they promote development of drug-resistance,
263 the bacteria-targeting strategies suggested by our *in silico* analysis counterintuitively promote
264 bacterial growth. However, these strategies would involve treatments, such as
265 immunosuppression (c_b decrease), that would be difficult to implement in reality because,
266 besides cytotoxicity and side-effects that immunosuppressive agents (e.g. cyclophosphamide)
267 cause, patients would be at risk of becoming susceptible to other infections.

268 Despite ample research focusing on the development of antimicrobial drugs, there is
269 surprisingly a large gap on the development of therapeutics that promote host defense during
270 infection (*29*). Such host-directed therapeutics are safer than pathogen-targeting drugs because
271 they promote the health of the host rather than attack the pathogen (*29*). Therefore, for our
272 experimental testing we singled out the category of k_b increase (namely T-cell activation and
273 recruitment). One of the most conventional and safe ways to boost k_b *in vivo*, which is also an
274 established, widely-used method for vaccine development, is via administration of inactivated
275 bacteria, namely antigens. Such treatment would be extremely practical in human therapeutics,
276 since pathogens causing renal abscesses in humans can be isolated from urine samples without
277 involving any invasive processes (*30*) and easily get inactivated. We chose inactivation of
278 bacteria with heat over toxic chemicals, such as formalin. Furthermore, heat-killed cells are more
279 effective, quicker to prepare and provide enhanced survival in treated animals than other
280 inactivation options (*31*). While inactivated bacteria in vaccines serve as prophylaxis from

281 infection, their use as treatment for ongoing chronic infections is limited. Here we explored
282 whether HK treatment during infection leads to cure, as our *in silico* results suggested.

283 Since our aim was to cure chronic *S. aureus* infection, the experimental perturbation (HK
284 treatment) had to be carried out when infection enters its chronic phase. As we have previously
285 shown, inoculation with $3–7\times10^7$ colony-forming units (CFU) of *S. aureus* results in chronic
286 infection and renal abscesses, and by day 14 of infection T cells are already strongly suppressed
287 by MDSCs (*5*, *6*). Therefore, the perturbation with HKSA was scheduled at day 14 after initial
288 infection with 5×10^7 CFU of *S. aureus*. The physiological k_b increase via HK treatment was
289 incorporated into the model with the addition of term k_bB_d to the T cells' ODE on the day of
290 treatment (*Materials and Methods*), where B_d the dose of HKSA and k_b the activation and
291 recruitment of T cells via HKSA assumed the same as for live bacteria during initial inoculation
292 (table S1). This assumption was based on the fact that, although live cells produce virulence
293 factors that stimulate the immune system, implying a greater value of k_b, heat-killed cells cannot
294 hijack or evade immunity as live *S. aureus* does. The only consequence of their existence in the
295 host is the stimulation of immune cells. Additionally, HKSA cells are injected when the host is
296 already chronically infected and had already encountered staphylococcal antigens during initial
297 inoculation. Secondary exposure to pathogens always initiates much stronger (and quicker)
298 immune response than the initial exposure to the same pathogen.

299 Numerical simulations for initial inoculation with 5×10^7 *S. aureus* cells and HK
300 treatment at day 14 of infection suggested that the minimum HKSA-dose required for cure would
301 be 4×10^7 HKSA (Fig. 2C). For our experiments, we opted for the amount of 10^8 HKSA. To
302 identify, on which day the infected mice would recover from infection to perform the

experimental sampling, we followed the *in silico* results, which predicted sterilizing immunity at day 34.5 of infection (Fig. 2D). Because biological systems involve extrinsic and intrinsic stochasticity and therefore not all infected mice are synchronized in the same infection phase, the experimental sampling was set at day 37 of infection (Fig. 2D). As a result of secondary exposure to *S. aureus*, HKSA-treatment initiates a cascade of inflammatory events, providing a concomitant, rapid boost in T-cell population (Fig. 2E, *brown*), which is followed by further, gradual increase of activated T cells as illustrated in our simulations (Fig. 2E). Consequently, HKSA-treatment destabilizes to a sufficient extent the system dynamics of chronic infection and leads to cure (Fig. 2D-2E).

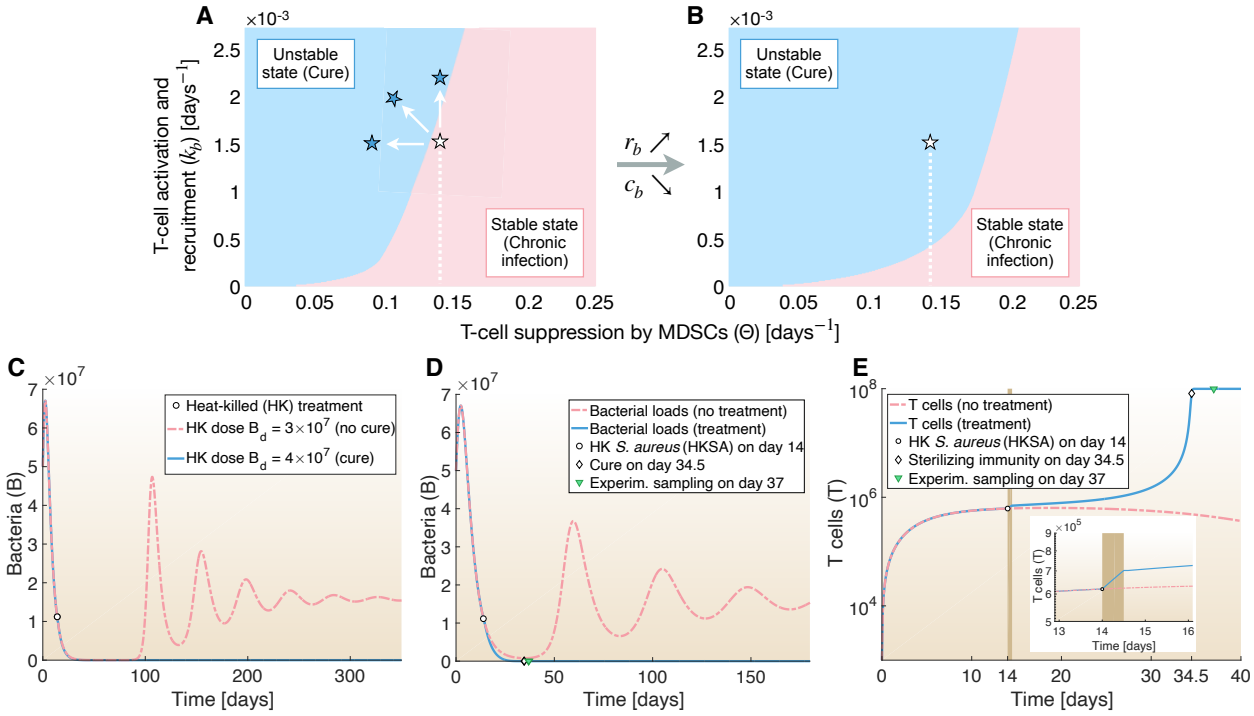

Fig. 2. Model-driven insights for cure. (**A-B**) Based on the eigenvalues of the ODE system, the phase diagram was divided into stable states (pink) and unstable states (blue), which represent the physiological chronic infection and cure, respectively. The white star represents the average position of an infected host during a chronic staphylococcal infection and was determined by the fitted values

317 of parameters k_b and Θ (table S1). Given the position of the infected host (white star), cure is
318 achieved (**A**) by increase of T-cell activation and recruitment (k_b) and/or decrease of T-cell
319 suppression by MDSCs (Θ) (shown as blue stars) or (**B**) by increasing the proliferation rate of
320 bacteria (r_b) and/or reducing the bacterial containment by T cells (c_b). (**C-E**) *In silico* treatment with
321 HKSA. Initial infection was induced by setting the bacterial population equal to 5×10^7 cells at day 0
322 in Eq. (1). T cells were set to 10^3 at day 0 in Eq. (2). HKSA-treatment was administered *in silico* at
323 day 14 of infection (shown as white bullet) by adding the term k_bB_d to the T-cell ODE at time
324 t=perturbation day, for a 12-hour perturbation window as explained in Eq. (3) (*Materials and*
325 *Methods*). (**C**) A minimum dose of HKSA for curing chronic *S. aureus* infection was estimated to be
326 $B_d = 4\times10^7$ HKSA. *In silico* administration of 10^8 HKSA, namely staphylococcal antigens, at day 14
327 of infection provides (**E**) quick boost of T cells (increase of parameter k_b), as shown in brown, and
328 (**D**) bacterial numbers are diminished to zero. Chronic *S. aureus* infection is cured.

329

330 ***In vivo* cure after model-driven perturbation treatment with HKSA**

331 Our next step was to provide proof-of-concept by validating our *in silico* predictions of cure *in*
332 *vivo*. For this purpose, C57BL/6 mice were infected intravenously with *S. aureus* strain SH1000.
333 At day 14 of infection mice were treated intraperitoneally with HKSA, strain SH1000. Control
334 mice received phosphate-buffered saline (PBS) (Fig. 3A).

335 Our previous study in chronically *S. aureus* SH1000-infected C57BL/6 mice has shown
336 that *S. aureus* is progressively depleted from multiple organs and persists only in the kidneys (*5*).
337 Therefore, at day 37 of infection, bacterial load quantification was performed in mice's kidneys.
338 The mathematical model's predictions *in silico* (Fig. 2D) were validated by our experiments *in*

339 *vivo*: mice treated with HKSA were cured with success percentage of 100% and no *S. aureus* at
340 all was found in their kidneys (Fig. 3B). In contrast, the majority of untreated animals remained
341 infected with high bacterial burden (Fig. 3B).

342 Progression of *S. aureus* infection from acute to chronic drives spleen T cells into T-cell
343 dysfunction, which we previously found irreversible (*5*). T-cell dysfunction during chronic *S.*
344 *aureus* infection is caused by the expansion and suppressive effect of all three MDSC subsets in
345 spleen (*6*, *13*). Therefore, at day 37 of infection, we next investigated the effect of the HKSA-
346 treatment on the proliferative response of T cells and on the MDSC populations. We found that
347 HKSA-treatment restored the function of spleen T cells. Stimulation with anti-CD3/anti-CD28
348 antibodies showed that T cells were hyperresponsive and actively proliferated (Fig. 3C). In
349 contrast, spleen T cells of infected untreated animals remained hyporesponsive to TCR re-
350 stimulation (Fig. 3C). We further observed significant reduction of all MDSC subsets in spleens
351 of HKSA-treated mice, whereas MDSC populations remained high in spleens of infected,
352 untreated (control) animals, which had received PBS (Fig. 3D). Together, these findings reveal
353 that HKSA-treatment during chronic *S. aureus* infection not only boosts T-cell function (namely
354 *in vivo* k_b increase) but also has a previously unidentified potential to indirectly target the
355 MDSCs (namely *in vivo* Θ decrease). Because MDSC-expansion and MDSC-mediated
356 suppression on T cells are associated with the chronic but not acute phase of the infection (*5*, *6*,
357 *8*), these results suggest that acute inflammation caused by administration of HKSA (see below)
358 disrupts the balance of chronic infection, which sustains MDSCs, leading to natural MDSC-
359 depletion.

360

361 **HKSA-treatment during chronic *S. aureus* infection induces strong acute inflammation**

362 Our *in silico* analysis suggested that destabilizing the system of chronic *S. aureus* infection by
363 administering a sufficient amount of HKSA would lead to cure. It was natural to expect that the
364 insertion of staphylococcal antigens into the hosts via HKSA-injection would trigger acute
365 inflammation. To verify *in vivo* that the HKSA-injection initiated acute inflammation during
366 chronic *S. aureus* infection, we sampled peritoneal exudates 12 hours after intraperitoneal
367 HKSA-treatment and assessed differences in populations of macrophages, as well as infiltrating
368 monocytes and granulocytes compared to untreated mice. It has been previously shown that two
369 distinct subsets of macrophages exist in mouse peritoneal cavity (PerC), the $CD11b^{hi}F4/80^{hi}$
370 large peritoneal macrophages (LPMs) and the $CD11b^{+}F4/80^{low}$ small peritoneal macrophages
371 (SPMs), and together are responsible for most of phagocytosis happening in PerC (*32*, *33*).
372 Under normal physiological conditions, LPMs are the predominant macrophage subset in PerC
373 (*32*). However, under inflammatory conditions, the PerC environment changes drastically: LPMs
374 disappear and SPMs become the major subset along with substantial recruitment of SPM-
375 precursors, the $CD11b^{+}Ly6C^{+}$ monocytes (*32*) and of $CD11b^{+}Ly6G^{+}$ granulocytes
376 (neutrophils). In accordance, we observed massive increase in amounts of $CD11b^{+}Ly6C^{+}$
377 monocytes and $CD11b^{+}Ly6G^{+}$ granulocytes (neutrophils) in PerC of HKSA-treated mice
378 compared to untreated (control) mice (Fig. 3E). LPMs were the predominant macrophage subset
379 in chronically *S. aureus*-infected, untreated mice, indicating homeostatic conditions in PerC,
380 whereas treatment of chronically *S. aureus*-infected mice with HKSA resulted in disappearance
381 of LPMs and predominance of SPMs, indicating acute inflammation (Fig. 3E). Total number of
382 MΦ (LPMs plus SPMs) was increased in PerC of HKSA-treated mice (Fig. 3E). These results

383 suggest that treatment with HKSA during chronic *S. aureus* infection induced strong acute

384 inflammatory responses.

385

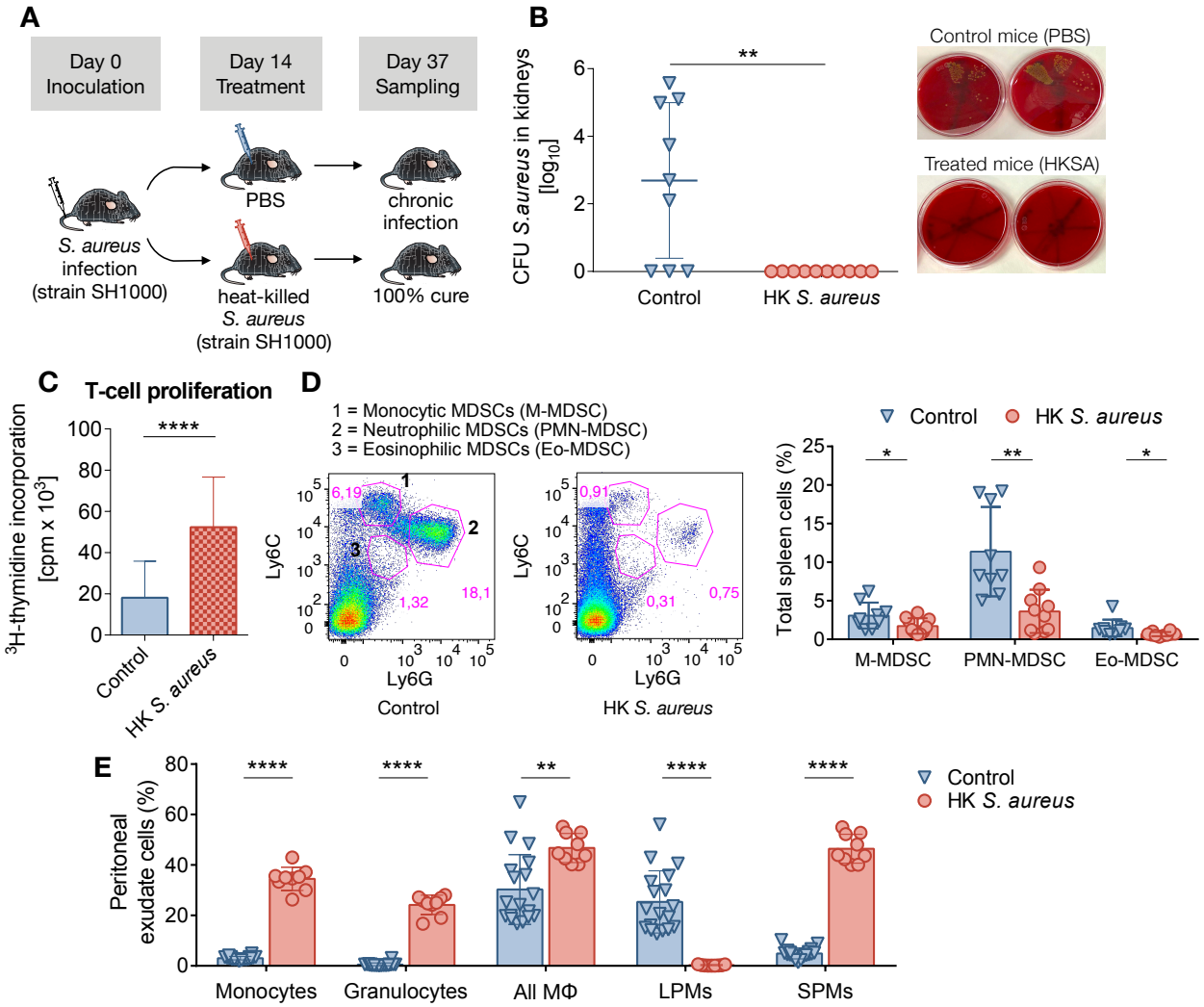

386

387 **Fig. 3. Bacterial burden and immune cells after treatment with heat-killed *S. aureus*.**

388 (**A**) Experimental schema. C57BL/6 mice were intravenously inoculated with 5×10^7 CFU of *S.*

389 *aureus* and intraperitoneally treated with 10^8 HKSA at day 14 of infection. Untreated (control) mice

390 received PBS. Sampling was conducted at day 37 of infection.

391 (**B**) Treatment with HKSA at day 14 of infection cures all chronically *S. aureus*-infected mice.

392 Bacterial loads were determined in kidneys of untreated (control) and HKSA-treated mice at day 37

393 of infection. n=4-5 mice per group, two independent experiments. Data represent mean±SD.
394 **p=0.0018, Student's t-test. Right: Representative images of ten-fold serial dilutions on blood agar
395 plates for enumeration of viable *S. aureus* (golden-yellow colonies) in kidney homogenates from
396 control (untreated) or HKSA-treated mice, showing high bacterial burden (bacterial persistence) or
397 absence of bacteria (bacterial eradication), respectively.
398 (**C**) Proliferative response of spleen T cells at day 37 of infection from chronically *S. aureus*-infected
399 mice which received PBS or HKSA to *in vitro* stimulation with anti-CD3/anti-CD28. T-cell
400 proliferation was measured by ^{3}H-thymidine incorporation. n=4-5 mice per group, two independent
401 experiments. Data represent mean counts per minute (cpm) ± SD. ****p<0.0001, Student's t-test.
402 (**D**) HKSA-treatment reduces MDSCs. (left) Representative fluorescence-activated cell sorting
403 (FACS) illustrating monocytic CD11b^{+}Ly6C^{+}Ly6G^{low}, neutrophilic CD11b^{+}Ly6C^{low}Ly6G^{+} and
404 eosinophilic CD11b^{+}Ly6C^{low}Ly6G^{low} MDSCs, and (right) percentage of each MDSC subset
405 within the total spleen cell population of untreated (control) or HKSA-treated mice at day 37 of
406 infection. n=4-5 mice per group, two independent experiments. Data represent mean±SD. *p<0.05
407 and **p<0.01, Student's t-test.
408 (**E**) Intraperitoneal HKSA-treatment at day 14 of infection induces acute inflammation. Peritoneal
409 exudate cells were collected from chronically *S. aureus*-infected mice 12 hours after administration
410 of PBS (control) or HKSA. Percentage of CD11b^{+}Ly6C^{+} monocytes, CD11b^{+}Ly6G^{+} granulocytes,
411 CD11b^{hi}F4/80^{hi} LPMs, CD11b^{+}F4/80^{low} SPMs along with total MΦ population (LPMs plus
412 SPMs) within the total peritoneal cell population is shown. n=5-10 mice per group, two independent
413 experiments. Data represent mean±SD. **p<0.01, ****p<0.0001, Student's t-test.

414

415 **Non-antigen-specific HK treatment**

416 The mathematical model suggested that treatment with HK *S. aureus* would cure chronic *S.*
417 *aureus* infection. Because MDSCs during chronic *S. aureus* suppress T cells, including antigen-
418 specific T cells, we proceeded to assess experimentally whether the HK treatment (perturbation
419 strategy) works in an antigen-specific manner. For reliable comparison with the experiments
420 using HKSA, we maintained the experimental design of the aforementioned quantified HKSA-
421 protocols (namely same CFU of *S. aureus* for inoculation, HK-dose, routes of administration,
422 times of treatment and sampling) and only replaced HKSA with HK cells of a different
423 bacterium. Therefore mice were inoculated with 5×10^7 *S. aureus*, however, they were treated
424 intraperitoneally with 10^8 HK *Streptococcus pyogenes* at day 14 of infection. Sampling was
425 performed at day 37 of infection (Fig. 4A). HKSP-treatment successfully cured 50% of
426 chronically *S. aureus*-infected mice (Fig. 4B), whereas the majority of control mice remained
427 infected. Similarly to experiments with HKSA-treatment, we explored how HKSP-treatment
428 affected T-cell proliferation and MDSC populations. Spleen T cells of HKSP-treated mice
429 responded to stimulation with anti-CD3 plus anti-CD28 antibodies and proliferated significantly
430 more than spleen T cells of untreated mice, which remained hyporesponsive (Fig. 4C). In
431 contrast to HKSA-treatment that led to considerable MDSC-depletion, the reduction of MDSCs
432 in HKSP-treated mice was insignificant compared to MDSCs in untreated mice (Fig. 4D).

433 As in the case of HKSA-treatment, peritoneal exudates were sampled 12 hours after
434 HKSP-treatment and confirmed acute inflammation. $CD11b^+Ly6C^+$ monocytes and
435 $CD11b^+Ly6G^+$ granulocytes (neutrophils) increased massively in PerC of HKSP-treated mice
436 compared to untreated mice (Fig. 4E). LPM-disappearance further confirmed acute inflammation
437 induced by HKSP-treatment along with significant increase of SPMs (Fig. 4E). It is important to

438 note that after HKSA-treatment, which cured all infected hosts, $CD11b^+Ly6C^+$ monocytes
439 increased massively, whereas after HKSP-treatment, which cured half of the infected hosts,
440 $CD11b^+$ $Ly6G^+$ granulocytes (neutrophils) increased massively (Fig. 4E).

441 These results confirmed that HK treatment with either *S. aureus* or *S. pyogenes* induces
442 acute inflammation during chronic *S. aureus* infection. However, it was expected that HKSA-
443 treatment would initiate stronger acute inflammation than HKSP-treatment, because HKSA was
444 a re-exposure to *S. aureus*, while HKSP-treatment was a first-time exposure to *S. pyogenes*
445 antigens. This is reflected by a significant increase of total MΦ (LPMs plus SPMs) in PerC after
446 HKSA but not after HKSP-treatment compared to control, untreated mice (Fig. 4E). Weaker
447 acute inflammation after HKSP- than HKSA-treatment was also indicated by less reduction of
448 MDSCs in spleens (Fig. 3D, 4D), which are sustained in conditions of chronic (but not acute)
449 inflammation (*8*) in addition to almost twofold lower proliferative response of spleen T cells in
450 HKSP-treated compared to HKSA-treated mice (Fig. 3C, 4C). These results combined can
451 explain cure in 50% of HKSP-treated animals in comparison to cure in 100% of HKSA-treated
452 animals and accord with previous studies, suggesting that monocytes and macrophages promote
453 *S. aureus* clearance (*26*) and that after antigen immunization in PerC, SPMs migrate to lymph
454 nodes where they activate T cells (*33*, *34*).

455 Because treatment with 10^8 HKSP induced weaker acute inflammation and T-cell
456 stimulation than treatment with 10^8 HKSA, we hypothesized that treatment with higher HKSP-
457 dose (more antigens) would naturally induce stronger acute inflammation (including more
458 $CD11b^+Ly6C^+$ monocytes and SPMs), hence more indirect depletion of MDSCs and more
459 activated T cells, leading to cure of all HKSP-treated mice. For this purpose, we reduced the

460 value of parameter k_b in the treatment term k_bB_d by two or three times to reflect the weaker T-cell
461 stimulation by HKSP compared to HKSA and estimated day of clearance for varying HKSP-
462 doses B_d administered at day 14 of infection. Our simulations suggested that if higher HKSP-
463 dose (>10^8) is administered, all HKSP-treated mice could be cured (namely 100% success) by
464 sampling day, day 37 of infection (fig. S2).

465 As commonly known, secondary exposure to antigens elicits a faster immune response,
466 meaning that HKSA-treatment, which was a re-exposure to staphylococcal antigens, triggered a
467 much faster immune response compared to HKSP-treatment, which was a first-time exposure to
468 streptococcal antigens. Therefore, for HKSP-dose the same as HKSA-dose, HKSP-treatment
469 would require longer time to induce immune response relatively as strong as that induced by
470 HKSA. Consequently, although the cure of 50% of HKSP-treated mice at day 37 of infection,
471 when experimental sampling was conducted, was not statistically significant (Fig. 4B), we
472 hypothesized that at a later time-point HKSP-treatment could eventually cure all hosts. For this
473 purpose, we reduced the value of parameter k_b in the treatment term k_bB_d by two or three times to
474 reflect the weaker T-cell stimulation by HKSP compared to HKSA and we estimated the day of
475 clearance for 10^8 HKSP (B_d) administered at day 14 of infection. Indeed, our simulations
476 suggested that if sampling is conducted approximately 10 days or later than day 37 of infection,
477 all HKSP-treated mice may be cured, namely 100% success (fig. S2).
478
479

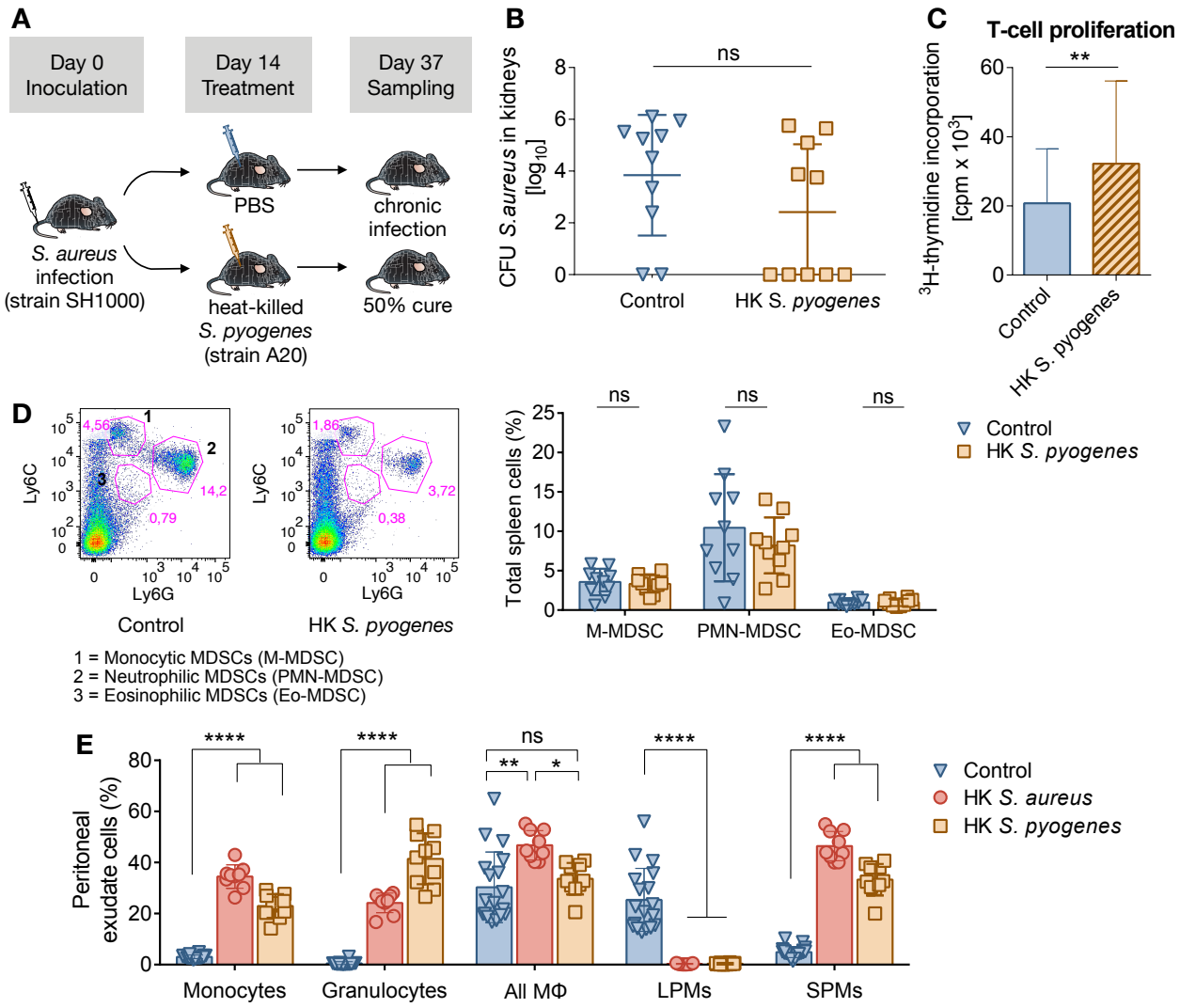

Fig.4. Bacterial burden and immune cells after treatment with heat-killed *S. pyogenes*.

(**A**) Experimental schema. C57BL/6 mice were intravenously inoculated with 5×10^7 CFU of *S. aureus* and intraperitoneally treated with 10^8 HKSP at day 14 of infection. Untreated (control) mice received PBS. Sampling was conducted at day 37 of infection.

(**B**) Treatment with HKSP at day 14 of infection cures 50% of chronically *S. aureus*-infected mice. Bacterial loads were determined in kidneys of untreated (control) and HKSP-treated mice at day 37 of infection. n=5 mice per group, two independent experiments. Data represent mean±SD, Student's t-test.

489 (**C**) Proliferative response of spleen T cells at day 37 of infection from chronically *S. aureus*-infected
490 mice which received PBS or HKSP to *in vitro* stimulation with anti-CD3/anti-CD28. T-cell
491 proliferation was measured by ^{3}H-thymidine incorporation. n=5 mice per group, two independent
492 experiments. Data represent mean counts per minute (cpm) ± SD. **p=0.0024, Student's t-test.
493 (**D**) HKSP-treatment slightly reduces MDSCs in spleen. Representative fluorescence-activated cell
494 sorting (FACS) illustrating monocytic $CD11b^{+}Ly6C^{+}Ly6G^{low}$, neutrophilic
495 $CD11b^{+}Ly6C^{low}Ly6G^{+}$ and eosinophilic $CD11b^{+}Ly6C^{low}Ly6G^{low}$ MDSCs (left), and percentage
496 of each MDSC subset within the total spleen cell population of untreated (control) or HKSP-treated
497 mice (right) at day 37 of infection. n=5 mice per group, two independent experiments. Data represent
498 mean±SD, Student's t-test.
499 (**E**) Intraperitoneal injection with HKSP at day 14 of infection induces acute inflammation.
500 Peritoneal exudate cells were collected from chronically *S. aureus*-infected mice 12 hours after
501 administration of PBS (control) or HKSP. Percentage of $CD11b^{+}Ly6C^{+}$ monocytes, $CD11b^{+}Ly6G^{+}$
502 granulocytes, $CD11b^{hi}F4/80^{hi}$ LPMs, $CD11b^{+}F4/80^{low}$ SPMs along with total MΦ population
503 (LPMs plus SPMs) within the total peritoneal cell population is shown. n=5-10 mice per group, two
504 independent experiments. Data represent mean±SD. *p<0.05, **p<0.01, ****p<0.0001, one-way
505 ANOVA with Tukey's multiple comparisons test. Peritoneal exudate cells collected 12 hours after
506 HKSA-treatment at day 14 of infection are included for comparison.

507

508 **Reasoning for past unsuccessful applications of the treatment**

509 Our model-driven protocol suggesting sufficient HKSA-dose, its administration day, and day of
510 complete bacterial clearance has proved reliable and effective for all HKSA-treated animals.
511 Although administration of inactivated cells as treatment for infections has been used in the past,
512 this kind of therapy is narrowly established. This is due to lacking information regarding the
513 sufficient dose(s) required and day(s) of administration that could resolve *S. aureus* infections
514 successfully. Until now, treatments with inactivated bacteria against *S. aureus* infections have
515 been based on vague experimental experience.

516 Here, we explain *in silico* why heat- or formalin-killed bacteria treatments used so far
517 have not been successful in yielding clearance. We base our arguments on a previous study (*35*),
518 in which scientists administered at least 19 injections with increased dose of formalin-killed *S.*
519 *aureus* over the period of 3 months in human patients with *S. aureus* infection (furunculosis).

520 In the study none of the chronically infected patients was reported to have attained
521 sterilizing immunity, even though they experienced moderate to strong clinical improvement.
522 The injecting scheme in the study consisted of increasing killed *S. aureus* doses (B_d) given in
523 intervals of 3-5 days as follows:

524 – Suspension I:$(0.1,0.2,0.3,0.4,0.5)\times 5\times 10^8$

525 – Suspension II: $(0.3, 0.4, 0.5, 0.6, 0.7, 0.8, 0.9, 1)\times 10^9$

526 – Suspension III:$(0.5,0.6,0.7,0.8,0.9,1)\times 2.5\times 10^9$.

527 We assumed that the bacterial capacity in humans is 1000 times greater than the bacterial
528 capacity in mice (based on the kidney weight ratio between mice and humans), created the
529 corresponding murine suspensions:

530 – Suspension IV:$(0.1,0.2,0.3,0.4,0.5)\times 5\times 10^5$

531 – Suspension V: $(0.3, 0.4, 0.5, 0.6, 0.7, 0.8, 0.9, 1)\times10^6$

532 – Suspension VI:$(0.5,0.6,0.7,0.8,0.9,1)\times2.5\times10^6$,

533 and applied them in our mouse model *in silico* every 4 days, starting from day 14, when chronic
534 infection is established in mice.

535 The conventional administration of injections with inactivated bacteria is based on the
536 belief that repeated vaccination could work more efficiently. Here, we employed *in silico* the
537 analogous protocol that has been administered in humans (suspensions IV-VI, 19 injections) and
538 showed that repeated injections with increasing doses of killed *S. aureus* cannot render
539 eradication of *S. aureus* (Fig. 5A). We also explored the case when not only more injections are
540 given (25 in total) but also with high fixed dose (almost fivefold higher than the highest dose of
541 suspensions IV-VI) and found that such treatments still fail to eliminate the infection (Fig. 5A).
542 Our results explicitly negate the current belief by showing that challenging the system of chronic
543 infection repeatedly with insufficient killed *S. aureus* dose and in high-frequency intervals does
544 not result in cure (Fig. 5A).

545 To gain a broader perspective on curative protocols, we simulated varying doses from
546 10^6 to 10^7 inactivated *S. aureus*, number of injections from 1-20 and time intervals between
547 injections from 0 up to 14 days (Fig. 5B-5D). Our *in silico* results suggested that for doses of 10^6
548 to 10^7 inactivated *S. aureus,* only treatment protocols involving HK injections with time
549 intervals from 1-3 days could cure (Fig. 5B, *blue*), with the maximum time interval of 3 days
550 requiring a minimum dose of 10^7 inactivated *S. aureus* to be effective (Fig. 5C). Therefore, both
551 the time intervals of 3-5 days and doses (suspensions IV-VI) analogous to as administered to
552 furunculosis patients (*35*) were fruitless attempts towards bacterial clearance, since the

553 administered doses in those time intervals were low to sufficiently stimulate the immune system
554 and lead to cure (Fig. 5B-5D). We next postulated that higher doses could have cured chronically
555 *S. aureus*-infected patients. For this purpose, we simulated curative and non-curative protocols
556 for varying number of injections, time intervals between injections and doses from 8×10^6 up to
557 10^8 inactivated *S. aureus*. Our results clearly indicated that higher doses could lead to cure (Fig.
558 6A-6C). Furthermore, our results showed that in case time intervals between injections need to
559 increase, (e.g. schedules of doctors), then higher HK-doses are required for cure (Fig. 6B).

560 Even though treatments with insufficient-for-cure doses of inactivated *S. aureus*, such as
561 the doses given to furunculosis patients, cannot confer complete clearance of bacteria,
562 furunculosis patients still reported improvement. In accordance, *in silico* administration of low
563 HK-doses showed that although they do not cure the hosts, they alleviate chronic infection by
564 providing remission (Fig. 6D). In fact, administration of HK treatment as early as possible leads
565 to longer remission of the infection (Fig. 6D). Lastly, we investigated how the administration
566 time of a HK-injection affects the clinical outcome. For middle-sized doses the day of
567 administration is crucial for the outcome of chronic infection, since it can provide cure if given
568 as early as possible or only provide temporary remission without clearing the infection (Fig. 6E).
569 These results highlight the urgency of treating chronic *S. aureus* infections as early as possible,
570 which is often compromised in cases of *S. aureus*-caused renal abscesses by improper and/or
571 time-consuming treatments (*16*, *30*).

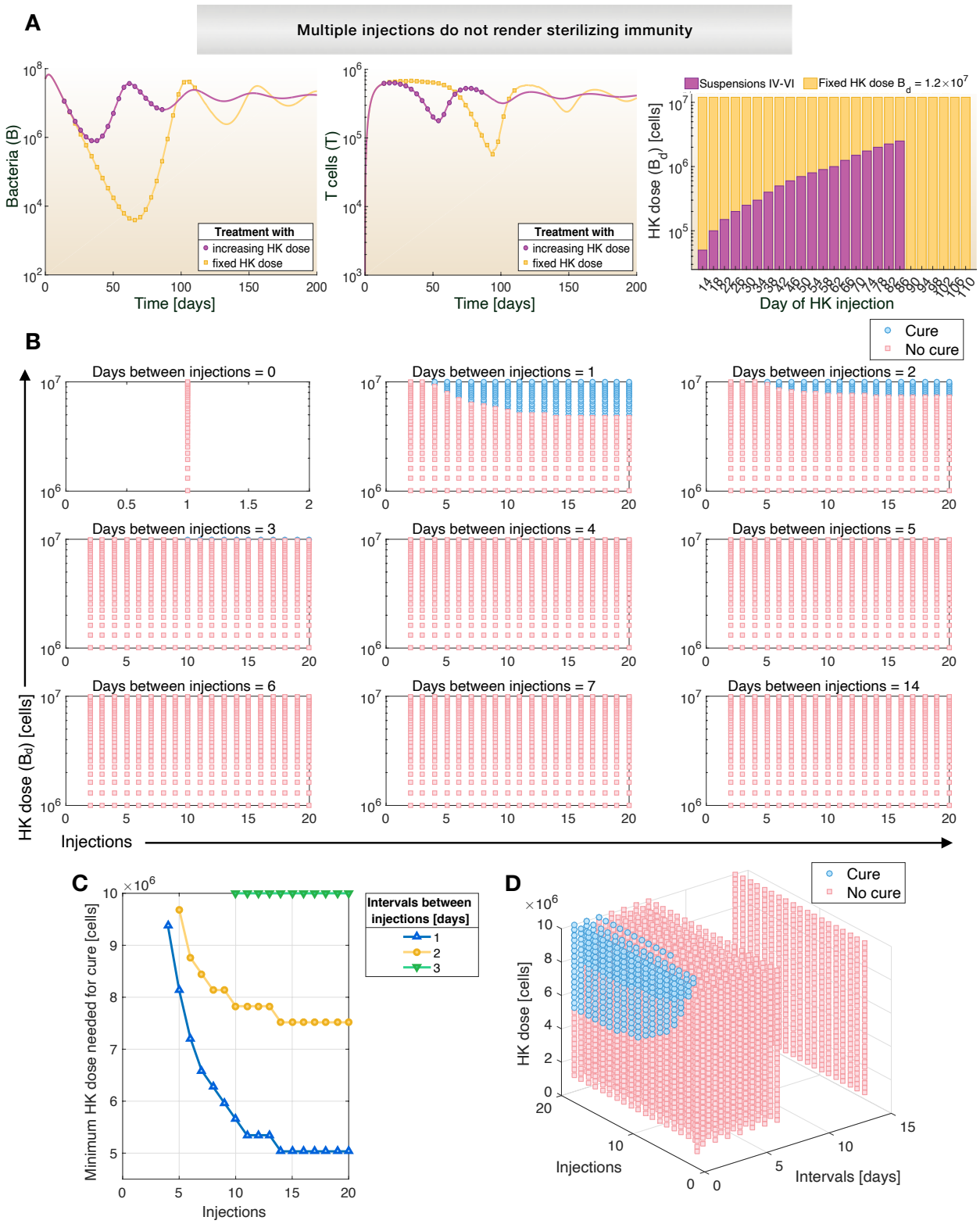

572

573 **Fig. 5. Simulations explain why previous treatments with inactivated *S. aureus* in humans were**

574 **unsuccessful and suggest curative treatment protocols.** At each injection day starting from day 14

575 of infection (when infection is chronic), treatment was incorporated into the T-cell ODE (Eq. (2)) as
576 $k_b B_d$, where k_b as defined in table S1 and B_d the varying, administered HKSA-dose. (**A**) Repeated
577 administration of inactivated *S. aureus* cannot render clearance. 19 HKSA-injections with increasing
578 dose in an analogous way to as administered in humans (suspensions IV-VI, purple) or 25 injections
579 with high fixed dose (yellow) were administered every four days. Chronic *S. aureus* infection
580 persists. (**B-D**) *In silico* predictions for cure plotted for 1 up to 20 HKSA-injections, HKSA-doses
581 ranging from 10^6 to 10^7, and time intervals between HKSA-injections from 0-7 days, or 2 weeks.
582 Time interval of 0 days means that only one HKSA-injection is administered. (**B**) Possibility of cure
583 declines when time intervals between HK-injections increase, even if many injections with high
584 HKSA-dose are administered. Each blue circle represents a unique, curative treatment protocol and
585 shows that cure is achieved only when time intervals between injections are 1-3 days with minimum
586 HKSA-dose needed for cure as in (**C**). (**D**) Interconnection between HKSA-doses 10^6 to 10^7,
587 HKSA-injections and time intervals between injections in three-dimensional plot.

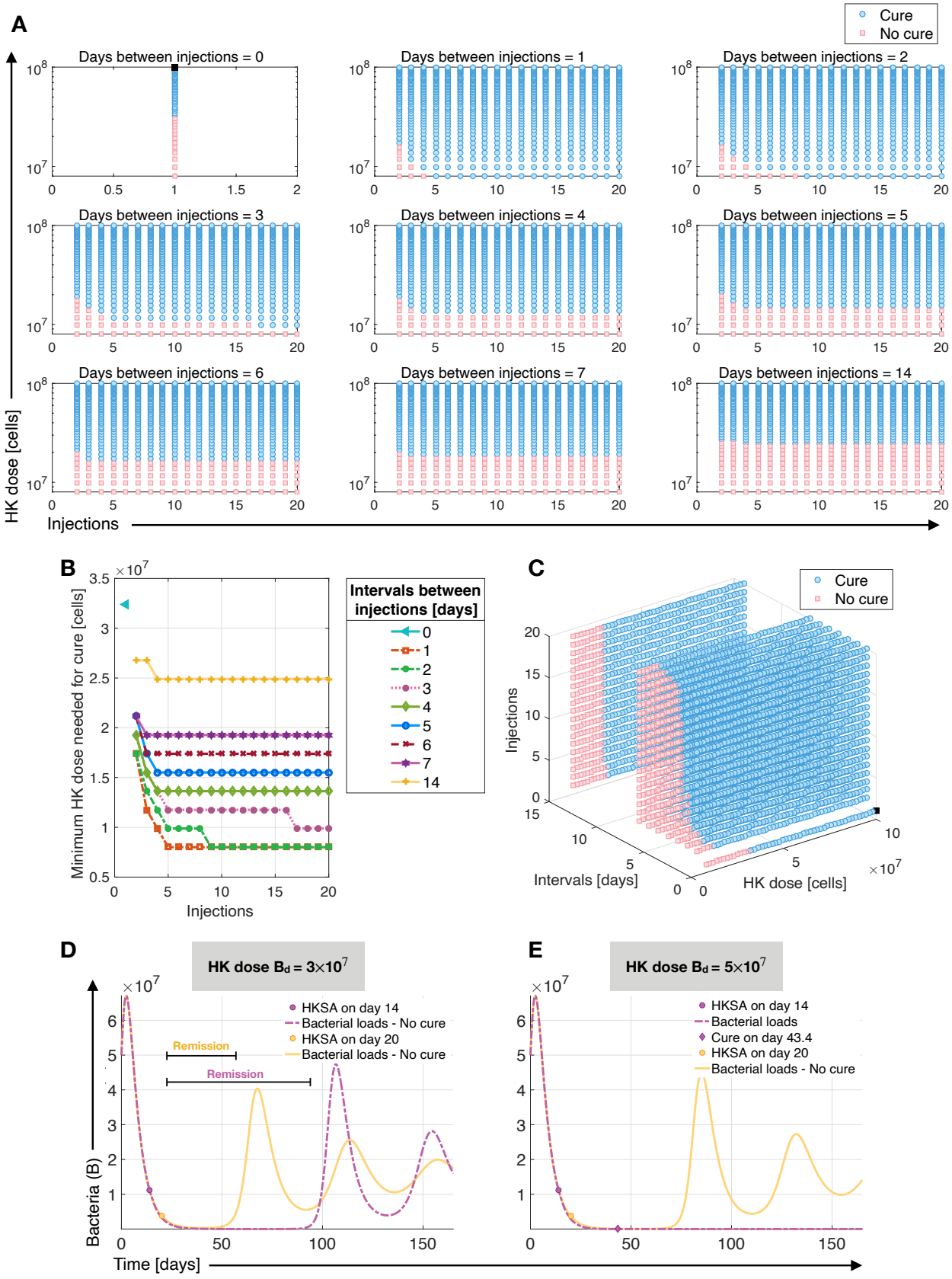
A
Cure
No cure
Days between injections = 0
Days between injections = 1
Days between injections = 2
Days between injections = 3
Days between injections = 4
Days between injections = 5
Days between injections = 6
Days between injections = 7
Days between injections = 14
HK dose [cells]
Injections
B
Minimum HK dose needed for cure [cells]
Injections
Intervals between injections [days]
0
1
2
3
4
5
6
7
14
C
Cure
No cure
Injections
Intervals [days]
HK dose [cells]
D
HK dose $B_d = 3\times10^7$
HKSA on day 14
Bacterial loads - No cure
HKSA on day 20
Bacterial loads - No cure
Remission
Remission
Bacteria (B)
Time [days]
E
HK dose $B_d = 5\times10^7$
HKSA on day 14
Bacterial loads
Cure on day 43.4
HKSA on day 20
Bacterial loads - No cure

588

589 **Fig. 6. *In silico* correlation between HKSA-doses from 8×10^6 to 10^8, number of HKSA-**
590 **injections and time intervals between injections for curative treatment protocols or remission.**
591 (**A-C**) Same as in Fig. 5B-5D for HKSA-doses ranging from 8×10^6 to 10^8. Each blue circle
592 represents a unique, curative treatment protocol, for which the minimum dose required for successful
593 treatment is indicated in (**B**). Black square in (**A**) and (**C**) represents the treatment protocol of 10^8
594 HKSA in a single injection that was tested experimentally in this study and cured all hosts *in vivo*.
595 (**D-E**) Influence of administration time of HKSA-injection on the chronic infection. The HKSA-
596 treatment *in silico* was added as term $k_b B_d$ to the T-cell ODE (Eq. (2)) at day 14 or 20 for a 12-hour
597 perturbation window, where k_b as in table S1 and B_d the HKSA-dose. Critical HKSA-dose required
598 for cure when administered at day 14 (early chronic infection) was estimated to be 4×10^7 (Fig. 2C).
599 Although lower HKSA-dose (**D**) for example $B_d = 3\times10^7$ HKSA cannot cure, it provides remission.
600 Higher HKSA-dose (**E**), such as $B_d = 5\times10^7$, confers sterilizing immunity when administered at early
601 timepoints of chronic infection but fails to cure when administered later, although it provides
602 remission temporarily.
603
604
605 **DISCUSSION**
606 At present, no treatment has proved to be completely effective in resolving chronic *S. aureus*
607 infections. There is no vaccine against *S. aureus* infections because all clinical trials have failed
608 (*36*). The development of new antibiotics would only be a temporary solution, until the
609 bacterium develops antibiotic resistance. Recent reports warn on the alarming increase of
610 antibiotic-resistant *S. aureus* infections in organs that have not been conventionally infected
611 before, including kidneys (*16*, *37*). Such reports highlight that treating infections in organs,

612 where the medical community is not traditionally used to encountering, is very challenging and
613 often misdiagnosed, therefore requiring prompt intervention once identified (*30*). Furthermore,
614 the current medical arsenal of antibiotics, MDSC-targeting drugs or surgery, is insufficient,
615 ineffective or inadvisable due to bacteria-resistance mechanisms, cytotoxicity of drugs, inability
616 to drain abscesses because of their location in internal organs or the high-risk medical status of
617 patients. Consequently, new, less complicated ways of treatment against *S. aureus* infections are
618 absolutely essential to find. We here reported cure of all chronically *S. aureus*-infected mice with
619 renal abscesses, using heat-killed *S. aureus* treatment, as quantified by our mathematical model.
620 Although inactivated *S. aureus* has been used to treat soft skin infections *(35)* this is, to our
621 knowledge, the first time heat-killed *S. aureus* is used to treat renal abscesses.

622 Conventional vaccination with inactivated microorganisms always requires multiple
623 doses to ensure prophylaxis. Hence, it is believed that inactivated microorganisms, when used as
624 treatment, should also be administered in multiple doses to be efficient (*35*). Here we provided
625 evidence that treatment with one HK-injection alone can cure chronic *S. aureus* infection (Fig.
626 2D, 3B). This is an important finding, because it means that a single injection with the right HK-
627 dose, besides being extremely practical to implement in human therapeutics, can suffice to break
628 the chronic phase of infection and lead to bacterial clearance, without the need for antibiotics,
629 that multidrug-resistant *S. aureus* can evade, or surgery for abscess drainage, or cytotoxic
630 MDSC-targeting drugs. Most importantly, pathogens causing renal abscesses in humans are
631 easily obtained without any invasive methods from urine samples from patients (*30*), which can
632 then be easily cultured and heat-killed. Regarding safety, the administration of inactivated *S.*
633 *aureus* as treatment of staphylococcal skin infection in human patients had only minor side-
634 effects, such as temporary pain at the site of injection (*35*). In accordance, our treatments with

635 HKSA or HKSP were well-tolerated. Treated animals did not exhibit any signs of side-effects or
636 discomfort. They were active, alert, observant of their environment, with eyes wide open, fur
637 laying flat and maintained normal body weight and appetite. Consequently, HK treatments bear
638 the potential to become easily produced, easily stored, cost-effective, and safe treatments in
639 medicine.

640 The recently identified Eo-MDSC inhibit, as other MDSCs, T-cell proliferation during
641 chronic *S. aureus* infection (*13*). Our results agree with previous results on the suppressive effect
642 of Eo-MDSC on T cells, since high Eo-MDSC numbers in control (untreated) mice contributed
643 to high T-cell suppression that was reduced as a result of reduced Eo-MDSC after HKSA-
644 treatment (Fig. 3C-3D). More Eo-MDSC have been directly linked with more CFU of *S. aureus*
645 (*13*). In accordance, our results showed that significant decrease of Eo-MDSC contributed to
646 bacterial clearance (Fig. 3B, 3D). Additionally, we here revealed a previously unidentified
647 approach for depletion of Eo-MDSC that was achieved in an indirect way, in contrast to
648 cytotoxic agents, which directly target MDSC-populations and bear side-effects.

649 Our mathematical model aimed to predict variables that could transition a chronic *S.*
650 *aureus* infection to an active inflammatory state to promote bacterial clearance. Our experiments
651 *in vivo* verified that perturbation with HKSA initiates acute inflammation during the chronic
652 establishment of *S. aureus* infection, showing massive increase in amounts of $CD11b^{+}Ly6C^{+}$
653 monocytes, $CD11b^{+}Ly6G^{+}$ granulocytes (neutrophils) and $CD11b^{+}F4/80^{low}$ SPMs in HKSA-
654 treated mice (Fig. 3E). Our previous study has shown that T cells from chronically *S. aureus*-
655 infected mice remained hyporesponsive after *in vitro* stimulation with either heat-killed *S. aureus*
656 or anti-CD3 plus anti-CD28 (*5*). This indicates that it is not the heat-killed treatment per se that
657 cured the infection, but rather the mathematically-driven concept of sufficiently destabilizing the

658 system dynamics *in vivo*. One of the strategies for destabilization of the chronic infection system,
659 as shown in this study, was achieved via administration of HKSA that caused acute inflammation
660 and subsequently created a new cascade of inflammatory events (including T-cell boost),
661 resulting in sterilizing immunity.

662 For the experiments regarding antigen-specificity of the treatment, *S. pyogenes* was
663 chosen because together with *S. aureus* they are the two most common gram-positive cocci of
664 medical significance (*38*). Delivery of 10^8 HKSP cleared *S. aureus* in 50% of animals,
665 suggesting that a portion of the effects of the HK treatment are antigen-independent and that a
666 non-antigen specific HK treatment may be completely effective if combined with other
667 perturbation strategies (antigen-specific or not). Even a higher HKSP-dose alone could have
668 potentially resolved the chronic infection in all HKSP-treated animals (fig. S2). Interestingly, we
669 found that other studies have used a similar approach to treat chronic *Mycobacterium*
670 *tuberculosis* infections with heat-killed *Mycobacterium vaccae,* especially in patients, in whom
671 previous treatment with antibiotics and/or chemotherapy had failed. Consistent with our results,
672 they also reported a therapeutic effect that cures patients (success percentages varying), along
673 with increase of T cells and an exemplary safety record even in patients co-infected with human
674 immunodeficiency virus (HIV). The copious advantages of heat-killed *M. vaccae* treatments led
675 to extensive Phase III clinical trials in patients in a plethora of countries around the globe (*39,*
676 *40*). Taking all the above into account, our results with *S. pyogenes* could be pioneer for chronic
677 *S. aureus* infections because they suggest that chronic *S. aureus* infections may be successfully
678 treated with other *S. aureus* strains or even other bacteria, for example *S. pyogenes*. If the
679 presented results are corroborated by further evidence and hold in human, a standardized cocktail
680 of the most frequent organisms causing renal abscesses can be added to hospital stocks for

681 immediate treatment of patients afflicted with renal abscesses. In addition, these results could
682 also help current efforts towards vaccine development for protection against *S. aureus*, since
683 antigens from other cocci/bacteria could be incorporated for vaccine testing.

684 Some diversity in the bacterial loads of control mice in all experiments *in vivo* was
685 observed (Fig. 3B, 4B). All control mice were infected with *S. aureus* but did not receive heat-
686 killed treatment. It was observed that in some of them *S. aureus* was cleared. Such variability can
687 be occasionally observed since (i) individual immune responses of mice can vary greatly and (ii)
688 biological systems are inherently stochastic. However, chronic infection and associated renal
689 abscesses caused by the same *S. aureus* strain as used here have been amply studied and the
690 dynamics of chronicity *in vivo* were published already years ago (*5*, *6*). Even though these
691 controls would be typically discarded, we included them for reasons of scientific transparency
692 and because this observed behaviour is explained mathematically in Fig. 2A: The average
693 position of an infected animal in the separatrix (*white star*) lies in the basin of attraction of
694 chronic infection (Fig. 2A, *pink area*) but is very close to the basin of attraction of cure (Fig. 2A,
695 *blue area*), indicating that a small portion of infected mice could spontaneously get cured.
696 Mathematically, points that lie close to the boundary separating two basins of attraction could
697 end up in the other attractor domain, namely the cure region, after stochastic perturbations
698 (possibly happening during the acute phase of the infection). Most essential is, however, the
699 effectiveness of the treatment because renal abscesses are often misdiagnosed, hence associated
700 with high risk of mortality (*30*), and once correct diagnosis takes place, the patients might
701 already experience organ damage and be in life-threatening conditions, whose lives could be
702 saved because of this treatment.

703 Our mathematical model is not limited to our proof-of-concept presented here. The
704 potential, novelty and usefulness of our mathematical model are further depicted in Fig. 6,
705 showing a plethora of unique, curative HKSA-treatment protocols with varying HK-doses,
706 number of HK-injections and time intervals between HK-injections (each blue bullet point). This
707 variety of quantified protocols can offer important flexibility for future treatments or clinical
708 trials because they can comply with the scientific and social circumstances, for instance working
709 hours of doctors, sensitivity of individuals to high HK-doses, or restrictions in animal permits.
710 We have started designing a graphical user interface for all these protocols, so that scientists can
711 choose HK-dose(s) or time intervals between treatment(s) and easily design their research and
712 treatments.

713 The results of this study are specified to C57BL/6 female mice; however, new *in silico*
714 curative protocols can be obtained when fitting the parameters of the mouse line or human of
715 interest. Most importantly, the simple structure of our model allows its easy adjustment for
716 chronic infections caused by other bacteria or staphylococcal strains, which could suggest
717 curative protocols against other strain- or bacteria-specific infections, including *S. aureus*
718 biofilms on medical implants that are devastating the clinics, renal abscesses caused by other
719 bacteria such as *Escherichia coli*, or infections in other internal organs. Future studies could be
720 such adjustment of model parameters for other bacteria or staphylococcal strains and subsequent
721 experiments based on model-driven treatment protocols for verification.

722 We here report cure of chronic *S. aureus* infection and renal abscesses without any use of
723 antibiotics, cytotoxic MDSC-targeting drugs, or surgical procedures for abscess drainage. Our
724 study provides proof-of-principle for a novel treatment protocol of chronic *S. aureus* infection by
725 repurposing heat-killed treatments, guided and quantified by our mathematical model. Unlike

726 conventional heat-killed administration, which is used as prophylaxis against infections in
727 humans and sometimes animals, we used this method as a treatment during ongoing chronic
728 infection. Treatments that are directed to promoting the immune response during an ongoing
729 infection are lacking. Our work could pave the way and provide a new scientific perspective
730 towards treatments that do not aim at targeting the infective agent (such as antibiotics), but rather
731 boost the host's own immune defense to resolve the infection.

732 METHODS

733 Mathematical model

734 The mathematical model was implemented and simulated in MATLAB, see
735 *www.mathworks.com*.

736 *Simulating the perturbation treatment*

737 To simulate the perturbation strategy, we incorporated, for a perturbation window of 12 hours,
738 the extra term $k_b B_d$ into the ODE describing T cells (Eq. (2)), where $B_d = 10^8$ cells is the dose of
739 heat-killed *S. aureus* and k_b = 0.001509 [days^{-1}] the parameter of T-cell activation and
740 recruitment as estimated during the fitting process (full description in Supplementary Materials;
741 table S1). The term of heat-killed treatment was incorporated into the ODE of T cells, because
742 heat-killed cells, as it happens when administered via conventional vaccines, deliver antigens
743 into the body that enhance the adaptive immunity. On each day (timepoint) of administration of
744 heat-killed treatment, such as day 14 of infection, the treatment term $k_b B_d$ was added, and the
745 equations became:

746 $$\dot{B}(t) = r_b B(t)\left(1 - \frac{B(t)}{\kappa}\right) - c_b T(t) B(t),$$

747 $$\dot{T}(t) = r_t T^2(t)\left(1 - \frac{T(t)}{K_T}\right) + k_b B(t) - c_T B(t) T(t) - \Theta\, T(t) + k_b B_d. \qquad (3)$$

748 Since heat-killed bacteria are not present continuously *in vivo*, the treatment term (that
749 simulates the *in vivo* conditions) was removed after the perturbation window and the equations
750 returned to their initial form as in equations (1)-(2). For treatment with heat-killed *Streptococcus*
751 *pyogenes* or varying HK-dose, the HK-dose B_d and value of k_b in the treatment term $k_b B_d$ were as
752 stated in the main text.

753

754 **Experimental protocols**

755 ***Bacteria***

756 *S. aureus* strain SH1000 *(41)* was grown to Mid-Log phase in brain heart infusion medium (BHI,
757 Roth, Karlsruhe, Germany) at 37°C with shaking (120 rpm), collected by centrifugation, washed
758 with sterile PBS, and diluted to the required concentration. The number of viable bacteria was
759 determined after serial diluting and plating on BHI-agar.

760

761 ***Mice and infection***

762 A previously described chronic renal abscess infection model (*5*) has been used in this study. It is
763 known that *S. aureus* strain SH1000 produces renal abscesses after intravenous inoculation (*5*).
764 Pathogen-free, 10 weeks-old C57BL/6 female mice were purchased from Harlan-Winkelmann
765 (Envigo, Netherlands). All animals were provided with food and water ad libitum, and housed in
766 groups of up to 5 mice per cage in individually ventilated cages. Statistical power analysis with
767 anticipated incidence of 10% and 90% for control and treated mice, respectively, indicated a
768 sample size of five mice per group. Mice were infected with 5×10^7 CFU of *S. aureus* in 100 µl of

769 PBS via a tail vein and monitored on a daily basis for weight loss and sign of pain or distress. At
770 specified times of infection, mice were sacrificed by CO_2 asphyxiation and the bacterial load was
771 enumerated in kidney homogenates by plating 10-fold serial dilutions on blood agar plates.
772 Spleens were removed, transformed in a single cell suspension and further processed for FACS
773 and proliferation assays.

774 In vaccination experiments, infected mice were injected intraperitoneally at day 14 of
775 infection with 10^8 heat-killed bacteria of *S. aureus* strain SH1000 or *S. pyogenes* strain A20 in
776 200 µl of PBS that were prepared by heating a bacterial suspension at 60°C for 1 h. At 12 h
777 postchallenge, mice were sacrificed and peritoneal exudate cells (PEC) were isolated from
778 infected mice by lavage of the peritoneal cavity with 2 ml sterile PBS. The lavage fluid was
779 centrifuged, supernatants stored at -20°C for subsequent cytokine analysis, and PEC resuspended
780 in complete RPMI, stained and analyzed by flow cytometry (see below).

781 Animal experiments were performed in strict accordance with the German regulations of
782 the Society for Laboratory Animal Science (GV-SOLAS) and the European Health Law of the
783 Federation of Laboratory Animal Science Associations (FELASA). All experiments were
784 approved by the ethical board Niedersächsisches Landesamt für Verbraucherschutz und
785 Lebensmittelsicherheit, Oldenburg, Germany (LAVES; permit N. 18/2798).

786

787 ***Flow cytometry analysis***

788 Cells were incubated with purified rat anti-mouse CD16/CD32 (BD Biosciences) for 5 min to
789 block Fc receptors and then stained with antibodies against CD11b (BioLegend), Ly6C
790 (BioLegend), Ly6G (Miltenyi Biotec), F4/80 (BD Biosciences) for 20 min at 4°C. Labeled cells

791 were measured by flow cytometry using a BDTM LSR II flow cytometer (BD Biosciences) and
792 analyzed by FlowJo software.
793
794 ***Proliferation assay***
795 Spleen cells were seeded into 96-well flat-bottom plates at 5 $\times 10^5$ cells/well in 100 μl of
796 complete RPMI medium and stimulated with 2 μg/ml of anti-CD3/anti-CD28 antibodies (Sigma-
797 Aldrich) at 37°C and 5% CO_2. After 3 days of incubation, the cells were pulsed with 1 μCi ^{3}H-
798 thymidine (Amersham) and harvested 18 h later on Filtermats A (Wallac) using a cell harvester
799 (Inotech). The amount of ^{3}H-thymidine incorporation was measured in a gamma scintillation
800 counter (Wallac 1450; MicroTrilux).
801
802 ***Statistical analyses***
803 All data were analyzed with GraphPad Prism Software. Comparisons between several groups
804 were made using a parametric ANOVA test with Tukey's multiple comparisons test. Comparison
805 between two groups was performed using a Student's t-test. P values <0.05 were considered
806 significant.
807

808 **Supplementary Materials for**

809 # Chronic *Staphylococcus aureus* infection is cured by theory-driven therapy

810 Lito A. Papaxenopoulou,* Gang Zhao, Sahamoddin Khailaie, Konstantinos Katsoulis-Dimitriou,
811 Ingo Schmitz, Eva Medina, Haralampos Hatzikirou,* Michael Meyer-Hermann*

812 *Corresponding author. Email: papaxenopoulou.lito@gmail.com;
813 haralampos.hatzikirou@ku.ac.ae; mmh@theoretical-biology.de

814

815 **The PDF file includes:**
816
817 Supplementary Methods
818 Fig. S1. Perturbation strategies suggest eradication of *S. aureus in silico*.
819 Fig. S2. Time of bacterial clearance for varying HK-doses and three values of T-cell
820 stimulatory parameter *in silico*.
821 Table S1. Model parameter values as used for model analysis.
822

823 **Other Supplementary Material for this manuscript includes the following:**

824 Table S2 (Microsoft Excel format). Raw experimental data.
825 MATLAB codes (zip file).

826

827 # Supplementary Methods

828 ## Mathematical model

829 The mathematical model was implemented and simulated in MATLAB, see
830 *www.mathworks.com*.

831

832 **Fitting curves and standard deviation of parameters**

833 The unknown parameters in the model were estimated in three steps. First, the carrying
834 capacity of bacteria $\varkappa$ was estimated based on our previously reported experimental results from
835 B and T cells-deficient RAG2$^{-/-}$ mice (only innate immunity present), which were initially
836 infected with 7×10^7 CFU of *S. aureus* strain SH1000 (same strain as used in the study here)
837 and showed a nearly constant level of *S. aureus* in kidneys from day 7 till day 56 (*5*). The mean
838 of these data points was taken as the bacterial carrying capacity. The carrying capacity of T cells
839 (parameter K_T) was assumed to be of the same order of magnitude as the bacterial carrying
840 capacity. Secondly, the growth rate of bacteria was estimated by solving the logistic growth
841 equation $\frac{dP}{dt} = rP\left(1 - \frac{P}{\kappa}\right)$ for r

842 $$r = \frac{ln\left(\frac{P(\kappa - P_0)}{P_0(\kappa - P)}\right)}{t}$$

843 where $\varkappa$ is the bacterial carrying capacity, P_0 is the initial inoculation number of bacteria and P is
844 the bacterial CFU at time t. Our previous experimental data showed that the bacterial loads in B
845 and T cells-deficient RAG2$^{-/-}$ mice reached 75% of the carrying capacity on day 2 and
846 fluctuated afterwards, after intravenous inoculation with 7×10^7 CFU of *S. aureus*. Assuming that

847 the bacterial load reached 75% of the carrying capacity by day 1 or day 2, we determined the
848 high and low boundary of r to be 0.636 and 0.318, respectively. The average of the low and high
849 boundary was taken as the bacterial growth rate r_b of the model. Finally, our previously reported
850 data of bacterial loads and absolute numbers of T cells in time from immunocompetent mice
851 with chronic *S. aureus* SH1000-infection and renal abscesses (*5*) were used to fit the rest of
852 unknown parameters. The fitting process used a Markov Chain Monte Carlo version of
853 Differential Evolution algorithm *(42)*. Parameter c_T, representing T-cell suppression locally (at
854 the site of infection which is the kidneys for the chronic infection here) appeared much smaller
855 than other parameters, in particular parameter Θ (representing T-cell suppression by MDSCs
856 systemically, namely distant from the site of infection, such as in spleen). We tested, in a second
857 study, the possibility of fitting the same data with $c_T = 0$. The fit quality remained the same;
858 therefore we concluded that c_T is zero and that the main T-cell suppression by MDSCs is exerted
859 systemically. This deduction accords with our previous experimental reports which showed
860 major T-cell suppression by MDSCs in spleens of mice that had chronic *S. aureus* infection in
861 kidneys (*6*, *13*). Fitted parameter values are shown in table S1.
862

863 **Scaling the model**

864 *For the analytical solutions and analytical stability analysis the calculations were made feasible*
865 *by using an analytically amenable ODE model, which approximates the original ODE as*
866 *described in Eq. (1)-(2).*

867 With the following change of variables we non-dimensionalize the ODE model (1)-(2):

868 $B = \beta_0 \xi, \qquad T = c_0 \psi, \qquad t = t_0 \tau.$

$$\Rightarrow \frac{dB(t)}{dt} = \frac{\beta_0 d\xi}{t_0 d\tau} = r_b\beta_0\xi - \frac{r_b}{\kappa}\beta_0^2\xi^2 - c_b c_0 \psi \beta_0 \xi$$

$$\Rightarrow \frac{d\xi}{d\tau} = r_b t_0 \xi - \frac{r_b}{\kappa} t_0 \beta_0 \xi^2 - c_b t_0 c_0 \xi \psi.$$

We impose that the coefficients of $\xi, \xi^2$and $\xi\psi$ are equal 1. Then

$$t_0 = \frac{1}{r_b}, \quad \beta_0 = \kappa, \quad c_0 = \frac{r_b}{c_b}. \tag{S1}$$

Therefore the new, non-dimensionalized equation for bacteria is

$$\frac{d\xi}{d\tau} = \xi - \xi^2 - \xi\psi \tag{S2}$$

For the equation $\dot{T}(t)$ we have the non-dimensionalized calculations:

$$\frac{dT(t)}{dt} = \frac{c_0 d\psi}{t_0 d\tau} = r_t c_0^2 \psi^2 + k_b \beta_0 \xi - c_T \beta_0 \xi c_0 \psi - \Theta c_0 \psi$$

$$\Rightarrow \frac{d\psi}{d\tau} = r_t t_0 c_0 \psi^2 - \Theta t_0 \psi - c_T \beta_0 t_0 \xi \psi + \frac{k_b \beta_0 t_0}{c_0}\xi$$

Substitution of the t_0, β_0 and c_0 (found in Eq. (S1)) gives the scaled equation for T:

$$\frac{d\psi}{d\tau} = \alpha\psi^2 + \beta\xi - \gamma\xi\psi - \delta\psi \tag{S3}$$

where $\alpha = \frac{r_t}{c_b}, \beta = \frac{\kappa k_b c_b}{r_b^2}, \gamma = \frac{\kappa c_T}{r_b}, \delta = \frac{\Theta}{r_b}.$ (S4)

Calculation of equilibrium points

From Eq. (S2) we have:

$\xi - \xi^2 - \xi\psi = 0 \Longrightarrow \xi = 0, and\ \xi = 1 - \psi$

- For $\xi = 0$ in Eq. (S3) we have:

$$\frac{d\psi}{d\tau} = 0 \Longrightarrow \alpha\psi^2 - \delta\psi = 0 \Longrightarrow \psi_1 = 0, and\ \psi_2 = \frac{\delta}{\alpha}$$

- For $\xi = 1 - \psi$ in Eq. (S3) in steady state we conclude that:

$$\psi_{3,4} = \frac{\beta + \gamma + \delta \pm \sqrt{[-(\beta + \gamma + \delta)]^2 - 4\beta(\alpha + \gamma)}}{2(\alpha + \gamma)} \qquad \text{(S5)}$$

Consequently the system has four equilibrium points in total:

- $(\xi_1, \psi_1) = (0,0)$
- $(\xi_2, \psi_2) = (0, \frac{\delta}{\alpha})$
- $(\xi_{3,4}, \psi_{3,4}) = (1 - \psi_{3,4}, \psi_{3,4})$ where $\psi_{3,4}$ is as shown above.

Existence of $\psi_{3,4}$

Equilibrium points $\psi_{3,4}$ exist only when $\Delta = (\beta + \gamma + \delta)^2 - 4\beta(\alpha + \gamma) \geq 0$, i.e. only when $\psi_{3,4}$ have no imaginary part. Equivalently

$$(\beta + \gamma + \delta)^2 - 4\beta(\alpha + \gamma) \geq 0$$

$$\beta^2 + \gamma^2 + \delta^2 + 2\beta\gamma + 2\beta\delta + 2\gamma\delta - 4\alpha\beta - 4\beta\gamma \geq 0 \qquad (\pm 4\beta\delta)$$

$$\beta^2 + \gamma^2 + \delta^2 - 2\beta\gamma - 2\beta\delta + 2\gamma\delta - 4\beta(\alpha - \delta) \geq 0$$

$$(-\beta + \gamma + \delta)^2 - 4\beta(\alpha - \delta) \geq 0 \qquad \text{(S6)}$$

According to the sign of the term $(\alpha - \delta)$ in condition (S6), we investigate when the equilibrium points $\psi_{3,4}$ exist.

- If $\alpha - \delta \leq 0 \Longrightarrow \delta \geq a$ then the equilibria $\psi_{3,4}$ exist.
- If $0 < \delta < \alpha$ then we reformulate Δ as follows:

$$\Delta = (-\beta + \gamma + \delta - 2\sqrt{\beta}\sqrt{\alpha - \delta}) \cdot (-\beta + \gamma + \delta + 2\sqrt{\beta}\sqrt{\alpha - \delta})$$

a) If $-\beta + \gamma + \delta \geq 0$ then for existence of $\psi_{3,4}$ we require $-\beta + \gamma + \delta - 2\sqrt{\beta}\sqrt{\alpha - \delta} \geq 0$. Then:

$$-\beta + \gamma + \delta - 2\sqrt{\beta}\sqrt{\alpha - \delta} \geq 0 \Longrightarrow \beta - (\gamma + \delta) + 2\sqrt{\beta}\sqrt{\alpha - \delta} \leq 0$$

$$\sqrt{\beta}^2 + 2\sqrt{\beta}\sqrt{\alpha - \delta} - (\gamma + \delta) \leq 0$$

$$\Longrightarrow \sqrt{\beta} \leq \frac{-2\sqrt{\alpha - \delta} \pm \sqrt{4(\alpha - \delta) - 4[-(\gamma + \delta)]}}{2}$$

$$\sqrt{\beta} \leq -\sqrt{\alpha - \delta} + \sqrt{\alpha + \gamma}$$

Note: The solution $\sqrt{\beta} \leq -\sqrt{\alpha - \delta} - \sqrt{\alpha + \gamma}$ is exempt because by definition $\sqrt{\beta} \geq 0$.

b) If $-\beta + \gamma + \delta \leq 0$ then for existence of $\psi_{3,4}$ we require $-\beta + \gamma + \delta + 2\sqrt{\beta}\sqrt{\alpha - \delta} \leq 0$. Then:

$$-\beta + \gamma + \delta + 2\sqrt{\beta}\sqrt{\alpha - \delta} \leq 0 \Longrightarrow \beta - (\gamma + \delta) - 2\sqrt{\beta}\sqrt{\alpha - \delta} \geq 0$$

$$\sqrt{\beta}^2 - 2\sqrt{\beta}\sqrt{\alpha - \delta} - (\gamma + \delta) \geq 0$$

$$\Longrightarrow \sqrt{\beta} \geq \frac{2\sqrt{\alpha - \delta} \pm \sqrt{4(\alpha - \delta) - 4[-(\gamma + \delta)]}}{2}$$

$$\sqrt{\beta} \geq \sqrt{\alpha - \delta} + \sqrt{\alpha + \gamma}$$

Note: The solution $\sqrt{\beta} \geq \sqrt{\alpha - \delta} - \sqrt{\alpha + \gamma}$ is trivially exempt.

Local stability analysis of equilibrium points

Jacobian Matrix J = $\begin{bmatrix} \frac{\partial \dot{\xi}}{\partial \xi} & \frac{\partial \dot{\xi}}{\partial \psi} \\ \frac{\partial \dot{\psi}}{\partial \xi} & \frac{\partial \dot{\psi}}{\partial \psi} \end{bmatrix} = \begin{bmatrix} 1 - 2\xi - \psi & -\xi \\ \beta - \gamma\psi & 2\alpha\psi - \gamma\xi - \delta \end{bmatrix}$

Evaluation of Jacobian matrix in the trivial equilibrium point (ξ_1, ψ_1):

J(0,0) = $\begin{bmatrix} 1 & 0 \\ \beta & -\delta \end{bmatrix} \Rightarrow |J(0,0)| = -\delta < 0$ (S7)

From linear algebra, it is known that if J is a 2×2 matrix and λ_1, λ_2 its eigenvalues, then the determinant of J, $|J| = \lambda_1 \times \lambda_2$. Since the determinant of the Jacobian matrix in Eq. (S7) is negative (i.e. det = $-\delta < 0$), it means that the eigenvalues are of a different sign, and hence the trivial equilibrium point is unstable (i.e. saddle point, which is always unstable).

For the equilibrium point $(\xi_2, \psi_2) = (0, \frac{\delta}{\alpha})$ we have:

$J(\xi_2, \psi_2) = \begin{bmatrix} 1 - \frac{\delta}{\alpha} & 0 \\ \beta - \gamma\frac{\delta}{\alpha} & 2\alpha\frac{\delta}{\alpha} - \delta \end{bmatrix} = \begin{bmatrix} 1 - \frac{\delta}{\alpha} & 0 \\ \beta - \frac{\gamma\delta}{\alpha} & \delta \end{bmatrix} \Rightarrow |J| = \delta \cdot \left(1 - \frac{\delta}{\alpha}\right)$ for the equilibrium point (ξ_2, ψ_2). The sign of the determinant depends on the term $\left(1 - \frac{\delta}{\alpha}\right)$. When $\delta > \alpha$, then $|J| < 0$ (hence one positive and one negative eigenvalue), meaning that the equilibrium point is saddle. This becomes unstable when $\delta < \alpha$. Next, we evaluate the Jacobian matrix in the equilibrium points $(\xi_{3,4}, \psi_{3,4})$, by using $\xi = 1 - \psi \geq 0$,

$$|J(1 - \psi, \psi)| = \begin{vmatrix} -1 + \psi & -1 + \psi \\ \beta - \gamma\psi & (2\alpha + \gamma)\psi - (\gamma + \delta) \end{vmatrix}$$

$$= -(-1 + \psi)(\beta + \delta + \gamma - 2(\alpha + \gamma)\psi)$$

$$= -(1-\psi)(2(\alpha+\gamma)\psi - (\beta+\delta+\gamma)).$$

We obtain the trace of the Jacobian matrix, tr(J), to determine the type of stability of equilibrium points $(\xi_{3,4}, \psi_{3,4})$,

$$tr(J) = -1 - \delta + \gamma(-1+\psi) + \psi + 2\alpha\psi = (1+2\alpha+\gamma)\psi - (1+\gamma+\delta).$$

We first need to find some critical values for ψ:

- If $|J(1-\psi, \psi)| = 0$, then

$$\psi_1^* = \frac{\beta+\gamma+\delta}{2(\alpha+\gamma)}. \quad \text{(S8)}$$

We know that the term $(1-\psi)$ equals ξ, which represents the bacteria, and hence $\xi = 1 - \psi \geq 0$.

- If $tr(J) = 0$, then

$$\psi_2^* = \frac{1+\gamma+\delta}{1+2\alpha+\gamma} \quad \text{(S9)}$$

From the critical points found in Eqs. (S8) and (S9), the stability of the equilibrium points $(\xi_{3,4}, \psi_{3,4}) = (1-\psi_{3,4}, \psi_{3,4})$ can be classified as follows:

Stable node or spiral (Represents the chronic phase):

- $|J| \geq 0 \;\; \Rightarrow \psi_1^* \leq (\beta+\gamma+\delta)/(2(\alpha+\gamma))$
- $\mathrm{tr(J)} \leq 0 \Rightarrow \psi_2^* \leq (1+\gamma+\delta)/(1+2\alpha+\gamma)$

$$\Rightarrow \psi^* \leq \min\{\psi_1^*, \psi_2^*\}$$

Saddle equilibrium point:

$$|J| < 0 \Rightarrow \psi_1^* > \frac{\beta+\gamma+\delta}{2(\alpha+\gamma)} \Rightarrow \psi^* > \frac{\beta+\gamma+\delta}{2(\alpha+\gamma)}$$

Unstable node or spiral:

- $|J| \geq 0 \Rightarrow \psi_1^* \leq \frac{\beta+\gamma+\delta}{2(\alpha+\gamma)} \Rightarrow \psi^* \leq \psi_1^*$
- $tr(J) \geq 0 \Rightarrow \psi_2^* \geq \frac{1+\gamma+\delta}{1+2\alpha+\gamma} \Rightarrow \psi^* \geq \psi_2^*$

$$\Rightarrow \frac{\beta+\gamma+\delta}{2(\alpha+\gamma)} \geq \psi^* \geq \frac{1+\gamma+\delta}{1+2\alpha+\gamma}.$$

However, since from fitting results (table S1) $c_T = 0$, we conclude that

$\psi_1^* = \frac{\beta+\delta}{2\alpha}$ and $\psi_2^* = \frac{1+\delta}{1+2\alpha}$.

Assuming $\Theta^* = \frac{r_t r_b}{c_b}$ and substituting α, β, and δ from Eqs. (S4),

$$\psi_2^* = \frac{1+\frac{\Theta}{r_b}}{1+\frac{2r_t}{c_b}} = \frac{r_b+\Theta}{r_b+2\Theta^*}.$$

Since ξ and ψ are normalized, ξ, ψ ≥ 0 and therefore $0 \leq \psi_1^*, \psi_2^* \leq 1$. Hence $\psi_2^* \leq 1$ resulting in

$$\Theta \leq 2\Theta^*. \qquad \text{(S10)}$$

Now, $\psi_1^* = \frac{\frac{\kappa\, k_b\, c_b}{r_b^2}+\frac{\Theta}{r_b}}{2\frac{r_t}{c_b}} = \frac{1}{2\Theta^*}\left(\frac{\kappa k_b r_t}{\Theta^*}+\Theta\right)$.

From Eq. (S10)

$$\psi_1^* \leq \frac{1}{2\Theta^*}\left(\frac{\kappa k_b r_t}{\Theta^*}+2\Theta^*\right) = 1+\frac{\kappa k_b r_t}{2(\Theta^*)^2} > 1.$$

As a consequence, ψ_1^* is rejected and the stability analysis for the equilibrium points $(\xi_{3,4}, \psi_{3,4}) = (1 - \psi_{3,4}, \psi_{3,4})$ can be updated as follows:

- ***Stable node or spiral (Represents the chronic phase):***

$$\psi^* \leq \psi_2^* \Rightarrow \psi^* \leq \frac{1 + \gamma + \delta}{1 + 2\alpha + \gamma}.$$

- ***Unstable node or spiral:***

$$\psi^* \geq \psi_2^* \Rightarrow \psi^* \geq \frac{1 + \gamma + \delta}{1 + 2\alpha + \gamma}.$$

Supplementary figures

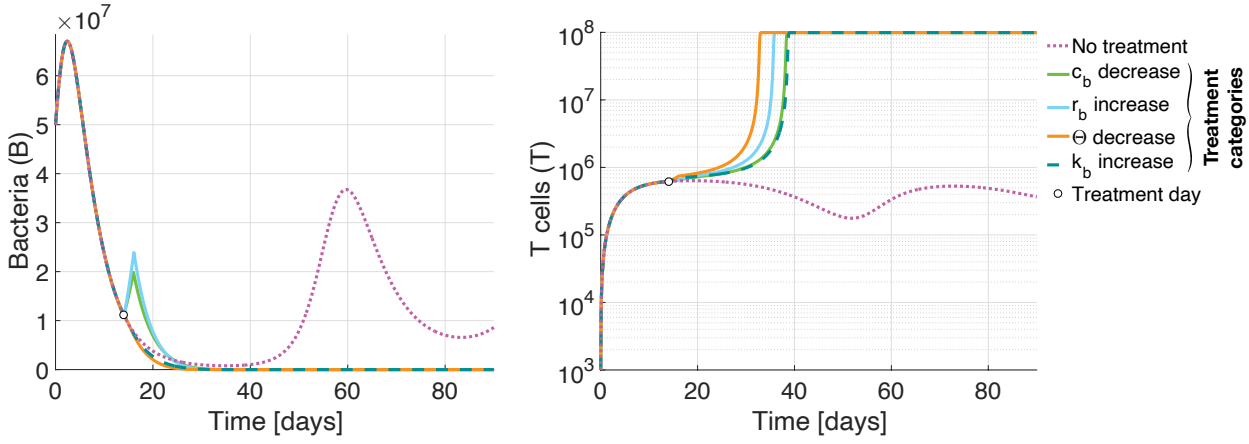

Fig. S1. Perturbation strategies suggest eradication of *S. aureus in silico*. Progression of *S. aureus* infection without any perturbation treatment results in a mathematically-characterized stable state and in a clinically-characterized persistent (chronic) *S. aureus* infection. When the chronic infection system is perturbed with treatments that (i) decrease host aggression against bacteria (c_b), for example via immunosuppressant drugs, (ii) increase bacterial growth (r_b), (iii) reduce MDSC-mediated immunosuppression (Θ), for instance via gemcitabine chemotherapeutic drug, or (iv) boosting adaptive immunity of the host (k_b), such as via administration of heat-killed bacterial antigens, *S. aureus* is eradicated and the host is cured. The plotted bacterial and T-cell dynamics in time are the numerical solutions of the ODE system (Eqs. (1)-(2)). Treatments were applied *in silico* at day 14 of infection (white bullet), namely when infection was already chronic, by decreasing or increasing the fitted value of the parameter of interest (table S1) for a perturbation window of 12 hours up to two days.

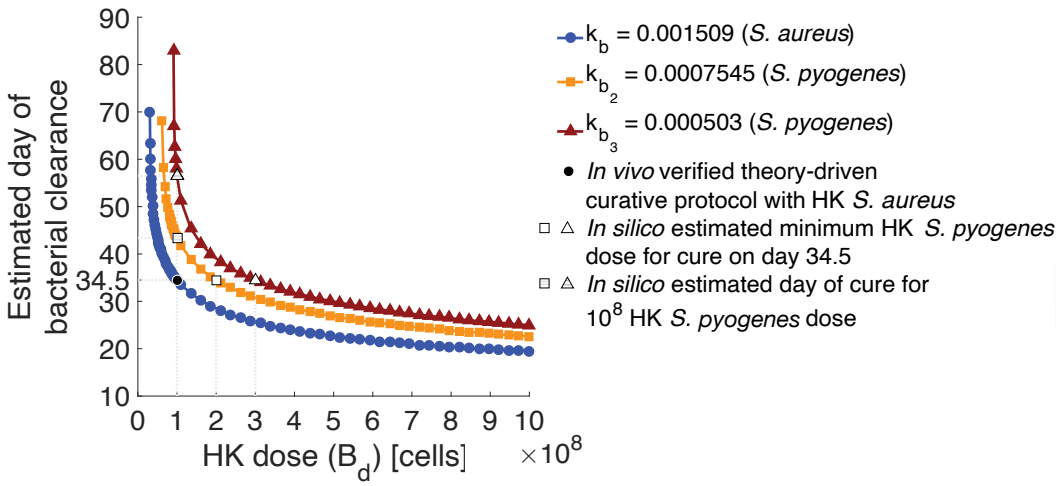

1011

1012 **Fig. S2. Time of bacterial clearance for varying HK-doses and three values of T-cell**

1013 **stimulatory parameter k_b *in silico*.** Stimulation of T cells by HK *S. aureus* cells at day 14

1014 happens with rate k_b = 0.001509 as defined during the fitting process (table S1). Since primary

1015 exposure to *S. aureus* already occurs upon inoculation at day 0, HK *Streptococcus pyogenes* at

1016 day 14 of infection stimulates the immune system at a weaker and slower rate compared to HK *S.*

1017 *aureus*, assumed as $k_{b2} = k_b/2 = 0.0007545$ or $k_{b3} = k_b/3 = 0.000503$. Simulation of HK treatments

1018 was done by adding the term $k_b B_d$ to the T-cell ODE at day 14 of infection for a perturbation

1019 window of half day (*Materials and Methods*), where k_b the immunostimulatory parameter

1020 varying for three different values (k_b, $k_b/2$, $k_b/3$) and B_d the HK-doses varying in the range

1021 $[4\times10^7, 10^9]$. The estimated day of clearance was defined as the first time-point when bacterial

1022 numbers <0.000001.

1023

1024 **Supplementary table**

1025

1026

1027 **Table S1. Model parameter values as used for model analysis.**

Parameter	Description	Value, [Confidence Interval]*	Unit
r_b	Bacterial growth rate (in the presence of innate immunity)	0.477	days^{-1}
$\varkappa$	Carrying capacity of bacteria	1.132×10^{8}	cells
c_b	Rate of bacterial containment by T cells (per cell)	9.937×10^{-7}, [8.65×10^{-7}, 1.25×10^{-6}]	days^{-1}
r_t	T-cell proliferation rate (per cell)	2.0955×10^{-7}, [1.04×10^{-7}, 2.94×10^{-7}]	days^{-1}
k_b	T-cell activation and recruitment rate	0.001509, [0.0011, 0.0017]	days^{-1}
c_T	Local T-cell suppression rate (per cell)	0	days^{-1}
Θ	Systemic MDSC-mediated suppression rate on T cells	0.14393, [0.072, 0.18]	days^{-1}
K_T	Carrying capacity of T cells	10^{8}	cells

1028 * In square brackets is the 95% confidence interval of the parameters as derived by a Markov Chain Monte Carlo

1029 version of Differential Evolution algorithm *(42)*.

1030

1031 **REFERENCES**

1032 1. L. Thomer, O. Schneewind, D. Missiakas, Pathogenesis of *Staphylococcus aureus*
1033 bloodstream infections. *Annu. Rev. Pathol. Mech. Dis.* **11**, 343-364 (2016).
1034 2. S. D. Kobayashi, N. Malachowa, F. R. DeLeo, Pathogenesis of *Staphylococcus aureus*
1035 abscesses. *Am. J. Pathol.* **185**, 1518-1527 (2015).
1036 3. B. L. Hahn, P. G. Sohnle, Direct translocation of staphylococci from the skin surface to deep
1037 organs. *Microb. Pathog.* **63**, 24-29 (2013).
1038 4. S. V. Kazakova, J. C. Hageman, M. Matava, A. Srinivasan, L. Phelan, B. Garfinkel, T. Boo,
1039 S. McAllister, J. Anderson, B. Jensen, D. Dodson, D. Lonsway, L. K. McDougal, M.
1040 Arduino, V. J. Fraser, G. Killgore, F. C. Tenover, S. Cody, A clone of methicillin resistant
1041 *Staphylococcus aureus* among professional football players. *N. Engl. J. Med.* **352**, 468-475
1042 (2005).
1043 5. C. Ziegler, O. Goldmann, E. Hobeika, R. Geffers, G. Peters, E. Medina, The dynamics of T
1044 cells during persistent *Staphylococcus aureus* infection: from antigen-reactivity to in vivo
1045 anergy. *EMBO Mol. Med.* **3**, 652-666 (2011).
1046 6. C. Tebartz, S. A. Horst, T. Sparwasser, J. Huehn, A. Beineke, G. Peters, E. Medina, A major
1047 role for myeloid-derived suppressor cells and a minor role for regulatory T cells in
1048 immunosuppression during *Staphylococcus aureus* infection. *J. Immunol.* **194**, 1100-1111
1049 (2015).
1050 7. M. Ost, A. Singh, A. Peschel, R. Mehling, N. Rieber, D. Hartl, Myeloid-derived suppressor
1051 cells in bacterial infections. *Front. Cell. Infect. Microbiol.* **6** (2016).
1052 8. E. Medina, D. Hartl, Myeloid-derived suppressor cells in infection: a general overview. *J.*
1053 *Innate Immun.* **10**, 407-413 (2018).

1054 9. C. Agrati, A. Sacchi, V. Bordoni, E. Cimini, S. Notari, G. Grassi, R. Casetti, E.
1055 Tartaglia, E. Lalle, D'Abramo, C. Castilletti, L. Marchioni, Y. Shi, A. Mariano, J.-W.
1056 Song, J.-Y. Zhang, F.-S. Wang, C. Zhang, G. M. Fimia, M. R. Capobianchi, M. Piacentini,
1057 A. Antinori, E. Nicastri, M. Maeurer, A. Zumla, Expansion of myeloid-derived suppressor
1058 cells in patients with severe coronavirus disease (COVID-19). *Cell Death Differ.* **27**, 3196-
1059 3207 (2020).
1060 10. E.-K. Vetsika, A. Koukos, A. Kotsakis, Myeloid-derived suppressor cells: major figures that
1061 shape the immunosuppressive and angiogenic network in cancer. *Cells* **8**, 1647 (2019).
1062 11. C. Guo, F. Hu, H. Yi, Z. Feng, C. Li, L. Shi, Y. Li, H. Liu, X. Yu, H. Wang, J. Li, Z. Li, X.-
1063 Y. Wang, Myeloid-derived suppressor cells have a proinflammatory role in the
1064 pathogenesis of autoimmune arthritis. *Ann. Rheum. Dis.* **75**, 278-285 (2016).
1065 12. O. Goldmann, E. Medina, *Staphylococcus aureus* strategies to evade the host acquired
1066 immune response. *Int. J. Med. Microbiol.* **308**, 625-630 (2018).
1067 13. O. Goldmann, A. Beineke, E. Medina, Identification of a novel subset of myeloid-derived
1068 suppressor cells during chronic staphylococcal infection that resembles immature
1069 eosinophils. *J. Infect. Dis.* **216**, 1444-1451 (2017).
1070 14. G. A. Noskin, R. J. Rubin, J. J. Schentag, J. Kluytmans, E. C. Hedblom, M. Smulders, E.
1071 Lapetina, E. Gemmen, The burden of *Staphylococcus aureus* infections on hospitals in the
1072 United States: an analysis of the 2000 and 2001 Nationwide Inpatient Sample Database.
1073 *Arch. Intern. Med.* **165**, 1756-1761 (2005).
1074 15. E. Y. Klein, W. Jiang, N. Mojica, K. K. Tseng, R. McNeill, S. E. Cosgrove, T. M. Perl,
1075 National costs associated with methicillin-susceptible and methicillin-resistant
1076 *Staphylococcus aureus* hospitalizations in the United States, 2010–2014. *Clin. Infect. Dis.*

1077 **68**, 22-28 (2018).

1078 16. F. Cedeira, F. Cedeira, E. M. Pagano, G. Castañeda, R. Rivadera, Bilateral nephrectomy as
1079 an extreme measure management for methicillin-resistant *Staphylococcus aureus* (MRSA):
1080 a case report. *Urol. Case Rep.* **33**, 101373 (2020).

1081 17. C. Hogea, T. Van Effelterre, C. J. Acosta, A basic dynamic transmission model of
1082 *Staphylococcus aureus* in the US population. *Epidemiol. Infect.* **142**, 468-478 (2014).

1083 18. E. McBryde, A. Pettitt, D.L.S. McElwain, A stochastic mathematical model of methicillin
1084 resistant *Staphylococcus aureus* transmission in an intensive care unit: predicting the
1085 impact of interventions. *J. Theor. Biol.* **245**, 470-481 (2007).

1086 19. W.-S. Choi, N. Son, J.-I. Cho, I.-S. Joo, J.-A. Han, H.-S. Kwak, J.-H. Hong, S. H. Suh,
1087 Predictive model of *Staphylococcus aureus* growth on egg products. *Food Sci. Biotechnol.*
1088 **28**, 913-922 (2019).

1089 20. A. Best, J. Jubrail, M. Boots, D. Dockrell, H. Marriott, A mathematical model shows
1090 macrophages delay *Staphylococcus aureus* replication, but limitations in microbicidal
1091 capacity restrict bacterial clearance. *J. Theor. Biol.* **497**, 110256 (2020).

1092 21. S. K. Shukla, T. C. Carter, Z. Ye, M. Pantrangi, W. E. Rose, Modeling of effective
1093 antimicrobials to reduce *Staphylococcus aureus* virulence gene expression using a two-
1094 compartment hollow fiber infection model. *Toxins* **12**, 69 (2020).

1095 22. M. Schmaler, N. J. Jann, F. Ferracin, R. Landmann, T and B cells are not required for
1096 clearing *Staphylococcus aureus* in systemic infection despite a strong TLR2–MyD88-
1097 dependent T cell activation. *J. Immunol.* **186**, 443-452 (2011).

1098 23. H. K. Kim, V. Thammavongsa, O. Schneewind, D. Missiakas, Recurrent infections and
1099 immune evasion strategies of *Staphylococcus aureus*. *Curr. Opin. Microbiol.* **15**, 92-99

1100 (2012).

1101 24. S. Khailaie, F. Bahrami, M. Janahmadi, P. Milanez-Almeida, J. Huehn, M. Meyer-
1102 Hermann, A mathematical model of immune activation with a unified self-nonself concept.
1103 *Front. Immunol.* **4**, 474 (2013).

1104 25. C. H. Kim, Homeostatic and pathogenic extramedullary hematopoiesis. *J. Blood Med.* **1**, 13
1105 (2010).

1106 26. C. E. Heim, D. Vidlak, T. D. Scherr, J. A. Kozel, M. Holzapfel, D. E. Muirhead, T.
1107 Kielian, Myeloid-derived suppressor cells contribute to *Staphylococcus aureus* orthopedic
1108 biofilm infection. *J. Immunol.* **192**, 3778-3792 (2014).

1109 27. C. Ma, T. Kapanadze, J. Gamrekelashvili, M. P. Manns, F. Korangy, T. F. Greten, Anti-Gr-1
1110 antibody depletion fails to eliminate hepatic myeloid-derived suppressor cells in tumor-
1111 bearing mice. *J. Leukoc. Biol.* **92**, 1199-1206 (2012).

1112 28. S. Ostrand-Rosenberg, P. Sinha, Myeloid-derived suppressor cells: linking inflammation
1113 and cancer. *J. Immunol.* **182**, 4499-4506 (2009).

1114 29. J. S. Ayres, Surviving COVID-19: a disease tolerance perspective. *Sci. Adv.* **6**, eabc1518
1115 (2020).

1116 30. K. A. Anderson, J. W. McAninch, Renal abscesses: classification and review of 40 cases.
1117 *Urology* **16**, 333-338 (1980).

1118 31. T. J. Yoon, J. Y. Kim, H. Kim, C. Hong, H. Lee, C.-K. Lee, K. H. Lee, S. Hong, S.-H.
1119 Park, Anti-tumor immunostimulatory effect of heat-killed tumor cells. *Exp. Mol. Med.* **40**,
1120 130-144 (2008).

1121 32. A. d. A. Cassado, M. R. D'Império Lima, K. R. Bortoluci, Revisiting mouse peritoneal
1122 macrophages: heterogeneity, development, and function. *Front. Immunol.* **6**, 225 (2015).

1123 33. E. E. B. Ghosn, A. A. Cassado, G. R. Govoni, T. Fukuhara, Y. Yang, D. M. Monack, K. R.
1124 Bortoluci, S. R. Almeida, L. A. Herzenberg, L. A. Herzenberg, Two physically,
1125 functionally, and developmentally distinct peritoneal macrophage subsets. *Proc. Natl.*
1126 *Acad. Sci. U.S.A* **107**, 2568-2573 (2010).
1127 34. E. Takenaka, A. Van Vo, Y. Yamashita-Kanemaru, A. Shibuya, K. Shibuya, Selective
1128 DNAM-1 expression on small peritoneal macrophages contributes to CD4+ T cell
1129 costimulation. *Sci. Rep.* **8**, 1-8 (2018).
1130 35. S. Holtfreter, J. Jursa-Kulesza, H. Masiuk, N. Verkaik, C. de Vogel, J. Kolata, M. Nowosiad,
1131 L. Steil, W. van Wamel, A. van Belkum, U. Völker, S. Giedrys-Kalemba, B. M. Broker,
1132 Antibody responses in furunculosis patients vaccinated with autologous formalin-killed
1133 *Staphylococcus aureus*. *Eur. J. Clin. Microbiol. Infect. Dis.* **30**, 707 (2011).
1134 36. D. Missiakas, O. Schneewind, *Staphylococcus aureus* vaccines: deviating from the carol.
1135 *J. Exp. Med.* **213**, 1645-1653 (2016).
1136 37. V. Vyas, T. Endy, A Rare case of prostatic and bilateral renal abscesses caused by
1137 community-acquired methicillin-resistant *Staphylococcus aureus* infection. *Cureus* **12**
1138 (2020).
1139 38. T. Fiedler, T. Köller, B. Kreikemeyer, *Streptococcus pyogenes* biofilms—formation,
1140 biology, and clinical relevance. *Front. Cell. Infect. Microbiol.* **5**, 15 (2015).
1141 39. J. Stanford, C. Stanford, J. Grange, Immunotherapy with *Mycobacterium vaccae* in the
1142 treatment of tuberculosis. *Front Biosci.* **9**, 1701–1719 (2004).
1143 40. M. I. Gröschel, S. A Prabowo, P.-J. Cardona, J. L. Stanford, T. S. Van der Werf.
1144 Therapeutic vaccines for tuberculosis—a systematic review. *Vaccine*. **32**, 3162–3168
1145 (2014).

41. M. Jonsson, S. Arvidson, S. Foster, A. Tarkowski, Sigma factor B and RsbU are required for virulence in *Staphylococcus aureus*-induced arthritis and sepsis. *Infect. Immun.* **72**, 6106-6111 (2004).

42. C. J. Ter Braak, A markov chain monte carlo version of the genetic algorithm differential evolution: easy bayesian computing for real parameter spaces. *Stat. Comput.* **16**, 239-249 (2006).

Acknowledgments: The authors thank Sabine Lehne and Lothar Gröbe for excellent technical assistance, and Drs. Anna Ntalli, Heiko Enderling, Andreas Papaxenopoulos, Yasmina Marin-Felix, Andreas I. Andreou and Kamila Tomoko Yuyama for useful comments on a draft of this article.

Funding: LP was supported by the German Federal Ministry of Education and Research within the initiative e:Med-network of systems-medicine, project MultiCellML (FKZ: 01ZX01707C). SK was supported by the German Federal Ministry of Education and Research within the Measures for the Establishment of Systems Medicine, project SYSIMIT (BMBF eMed project SYSIMIT, FKZ: 01ZX1308B and by the Helmholtz Association, Zukunftsthema "Immunology and Inflammation" (ZT-0027). GZ was supported by the Helmholtz Association within the initiative Immunology and Inflammation, project "Aging and Metabolic Programming" (AMPro). HH was supported by the Helmholtz Initiative on Personalized Medicine - iMed.

Author contributions: LP, HH, SK, GZ, and MMH designed the study, developed the methodology and interpreted the results. GZ performed the fitting process. LP performed the model implementation and simulations, and analyzed the results. LP and EM

designed and conducted the experiments. LP, KKD and IS analyzed the experimental results. HH and MMH supervised the study. All authors wrote the paper and approved the final version of the manuscript.

Competing interests: LP, GZ, SK, HH, and MMH are listed as inventors on pending patent (E.U. 19211206.8 - 1126, filed on 25th November 2019) related to the technology described in this work. The other authors declare no competing interests.

Data and materials availability: Original experimental data as well as MATLAB codes are provided in the manuscript or in the Supplementary Materials.